NJC

PAPER

View Article Online
View Journal | View Issue

Cite this: *New J. Chem.*, 2022, **46**, 18938

Visible-emitting Cu(I) complexes with *N*-functionalized benzotriazole-based ligands†

Jesús Castro, [a] Valentina Ferraro *[b] and Marco Bortoluzzi *[bc]

Luminescent mono- and dinuclear cationic heteroleptic Cu(I) complexes $[Cu(N\hat{}N')(P)_2]^+$, $[Cu(N\hat{}N')(P\hat{}P)]^+$ or $[Cu_2(N\hat{}N')_2(\mu\text{-}P\hat{}P)_2]^{2+}$ containing bidentate N-donor ligands (N^N′) with benzotriazole, pyridine, pyrimidine or substituted triazine moieties in combination with mono- (P) and bidentate (P^P) phosphines were synthesized and characterized. Eight single-crystal X-ray diffraction structures were obtained and showed marked distortions from the ideal tetrahedral geometry around Cu(I). Cyclic voltammetry on selected complexes showed reduction processes around −2 V *vs.* ferrocene/ferrocenium and irreversible oxidation close to 1 V. The long-wavelength absorptions were observed in the range of 350 to 450 nm and attributed to MLCT transitions. Upon excitation with near-UV and violet light, the complexes exhibited emissions from bright yellow (max 538 nm) to red (max 637 nm). Emission maxima, luminescence lifetimes and photoluminescence quantum yields that reach up to 0.92 on powder samples resulted in strong dependence on the choice of the coordinated ligands, the acceptor character of the N^N′ ligands in particular. DFT calculations confirmed the electrochemical and photophysical outcomes and strongly suggested that the emission has a metal-to-ligand charge transfer (MLCT) nature, with intersystem crossing affording triplet emitting states.

Received 27th June 2022,
Accepted 7th September 2022

DOI: 10.1039/d2nj03165e

rsc.li/njc

Introduction

Luminescent first-row transition metal complexes are viable alternatives to second- and third-row transition elements and trivalent lanthanide derivatives for advanced applications such as organic light-emitting diodes (OLEDs), light-emitting electrochemical cells (LECs), solar cells, and sustainable photoactivated reactions.[1–13] In particular, d-block metals such as Ir(III) and Pt(II) are commonly exploited in photoluminescent dyes for OLEDs,[14–18] but their high cost, scarce abundance and toxicity determined growing interest for cheaper and greener alternatives. Moreover, the employment of precious and rare-earth metals is geopolitically problematic because of the presence of only a few mining countries. The extraction and separation processes are highly energy- and water-consuming and sometimes require toxic chemicals.

In this context, Cu(I) complexes are considered a valid choice thanks to their photophysical properties, including the possibility of tuning the colour of the emission. The closed-shell d^{10} ground-state configuration circumvents the problem of efficient non-radiative deactivation of excited states *via* low-lying metal-centred states, as generally observed for several other 3d metal ions with a partially filled d-shell. Moreover, Cu(I) complexes can exhibit peculiar features ascribable to thermally activated delayed fluorescence (TADF), appealing for OLED technology thanks to the possibility of harvesting both singlet and triplet excitons.[19–24] Consequently, a maximum of 100% efficiency can be expected from exciton spin statistics, similar to precious metal-based phosphorescent OLEDs. In most of the cases luminescence is attributed to metal-to-ligand charge transfers (MLCT), where the excited state formally contains an oxidized metal centre and a reduced ligand. Small

[a] *Departamento de Química Inorgánica, Universidade de Vigo, Facultade de Química, Edificio de Ciencias Experimentais, 36310 Vigo, Galicia, Spain*
[b] *Dipartimento di Scienze Molecolari e Nanosistemi, Università Ca' Foscari Venezia, Via Torino 155, I-30172 Mestre (VE), Italy. E-mail: valentina.ferraro@unive.it, markos@unive.it*
[c] *Consorzio Interuniversitario Reattività Chimica e Catalisi (CIRCC), via Celso Ulpiani 27, 70126 Bari, Italy*

† Electronic supplementary information (ESI) available: Heteronuclear NMR spectra of the ligands, Fig. S1–S6; description of the X-ray structures of trz^{OMe}-btz and trz^{OPh}-btz; asymmetric units of trz^{OMe}-btz and trz^{OPh}-btz and superimposition, Fig. S7–S9; intermolecular interactions in trz^{OMe}-btz and trz^{OPh}-btz, Fig. S10 and S11; crystal data and structure refinement for trz^{OMe}-btz and trz^{OPh}-btz, Table S1; heteronuclear NMR spectra of the complexes, Fig. S12–S30; crystal data and structure refinement for complexes **1a** and **2a**, Table S2; ellipsoid plots of $[\mathbf{1a}]^+$ and $[\mathbf{2a}]^+$, best superimposition and π,π-stacking interaction in complex **2a**, Fig. S31–S33; crystal data and structure refinement for the complexes, Tables S3 and S4; ellipsoid plot of cations $[\mathbf{2b}]^+$, $[\mathbf{1d}]^+$, $[\mathbf{2c}]^{2+}$, $[\mathbf{3b}]^+$, $[\mathbf{4d}]^+$ and $[\mathbf{5d}]^+$, Fig. S34; selected bond lengths [Å] and angles [°] for the complexes, Tables S5–S8; best superimposition of complexes **2a** and **2b**, Fig. S35; superimposition between free and coordinated ligands trz^{OPh}-btz in complex **5d**, Fig. S36; continuous shape measure calculation and other related parameters, Table S9; absorption spectra of complexes in 10^{-5} M CH_2Cl_2, Fig. S37. Cartesian coordinates of the DFT-optimized structures as separated .xyz file. CCDC 2100419–2100423, 2111460–2111464. For ESI and crystallographic data in CIF or other electronic format see DOI: https://doi.org/10.1039/d2nj03165e

modifications on the skeleton of the ligands can determine appreciable changes in photoluminescence, since the lowest unoccupied molecular orbital (LUMO) usually corresponds to a π^* orbital of the coordinated ligands.[25,26] Common N-donor ligands exploited for the preparation of luminescent Cu(I) complexes are polypyridines such as 1,10-phenanthroline and its derivatives, often combined with phosphines in a metal coordination sphere. Particular interest was devoted to the effects on the luminescence features of the extension of the π-delocalization in the N-donor chelates by the introduction of well-designed substituents. Moreover, the correlation existing between the bite angle of chelating phosphines and the energy of the MLCT absorption was investigated. Also, the intermolecular π-interactions at the ground state were revealed to influence the photoluminescence quantum yields.[27–34]

Recently, azoles proved to be promising building blocks for the synthesis of suitable ligands in the field of Cu(I) luminescent compounds. For instance, benzimidazole and its functionalized derivatives were extensively used.[35,36] The functionalization of azoles with other heterocycles or π-delocalized donor moieties is a common approach to simultaneously obtain rigid bidentate structures and remove high energy oscillators. An example is the straightforward isolation of a luminescent binuclear Cu(I) complex with a conjugate base of 4-*tert*-butylphenyl(pyrrole-2yl-methylene)amine starting from precursor $[Cu(NCCH_3)_4][BF_4]$.[37] A wide variety of further examples involving azoles from pyrazoles to tetrazoles was reported.[9,38–53] The four coordinated complex [Cu(bis(2-(diphenylphosphino)phenyl)ether)(5-(2-pyridyl)tetrazolate)] was deeply studied also from a computational point of view, focusing the attention on the ISC process.[54]

Despite its renowned versatility, benzotriazole is not commonly used as a ligand for the preparation of luminescent transition metal complexes.[55–57] Our research group recently exploited benzotriazole and the related heterocycle indazole as coordinating moieties in polydentate ligands applied for the preparation of luminescent Cu(I) complexes.[58–60]

So far, the conjugation of benzotriazole in combination with different aromatic N-donor heterocycles was not considered. Herein, we report the synthesis and characterization of bright yellow- and reddish orange-emitting Cu(I) complexes with bidentate ligands obtained by functionalization of the benzotriazole NH moiety with other heterocycles, in particular pyridine, pyrimidine and alkoxy-substituted triazines. The ligands and their acronyms are reported in Scheme 1 for clarity.

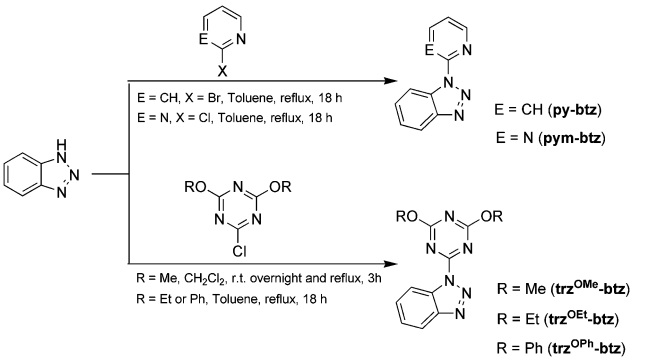

Scheme 1 Synthesis of *N*-functionalized benzotriazole-based ligands.

Results and discussion

Synthesis and characterization of the ligands

1-(Pyridin-2-yl)benzotriazole (py-btz) and 1-(pyrimidin-2-yl)benzotriazole (pym-btz) were obtained from methods previously reported by Katritzky and co-workers, based on the aromatic nucleophilic substitution of C-bonded halides by benzotriazole.[61,62] The triazinyl-benzotriazoles trz^{OMe}-btz, trz^{OEt}-btz and trz^{OPh}-btz were obtained by reacting the related 2-chloro-triazines with benzotriazole. The synthetic procedures, summarized in Scheme 1, are detailed in the Experimental section together with characterization data.

Mono- and bidimensional NMR spectra are collected in the ESI† (Fig. S1–S6). In the cases of 1-(4,6-dimethoxy-1,3,5-triazin-2-yl)benzotriazole (trz^{OMe}-btz) and 1-(4,6-diphenoxy-1,3,5-triazin-2-yl)benzotriazole (trz^{OPh}-btz), the formulae were further confirmed by single crystal X-ray diffraction obtained from slow evaporation of CH_2Cl_2 (trz^{OMe}-btz) or acetone (trz^{OPh}-btz) solutions. The description of the structures of trz^{OMe}-btz and trz^{OPh}-btz is reported in the ESI† (see also Fig. S7–S11 and Table S1).

Synthesis and characterization of the complexes

To obtain heteroleptic Cu(I) complexes with PPh_3 in the coordination sphere, all the ligands in Scheme 1 were coordinated by reaction of their conjugated acids (obtained *in situ* by adding $HBF_4{\cdot}Et_2O$) with $[Cu(\kappa^2\text{-}BH_4)(PPh_3)_2]$. The same synthetic approach using Cu(I) borohydride precursors with other phosphines[63] afforded multiple products; therefore, the synthesis of the other complexes prosecuted using $[Cu(NCCH_3)_4][BF_4]$ as a precursor. The acetonitrile complex was reacted with the proper phosphine, triisopropylphosphine P^iPr_3, 1,2-bis(diphenylphosphino)ethane dppe or bis[(2-diphenylphosphino)phenyl]ether DPEphos, and subsequently with the chosen chelating N-donor ligand. The procedures followed, sketched in Scheme 2 together with the numbering of the complexes and the yields, are detailed in the Experimental Section with the corresponding characterization data. ^1H and $^{31}P\{^1H\}$ NMR spectra are collected in the ESI† (Fig. S12–S30).

In all the cases, elemental analyses agree with the proposed formulae and conductivity measurements in acetone indicate that the complexes behave as 1 : 1 electrolytes, with the exception of the dinuclear dppe derivatives **1c–5c** (*vide infra*), acting as 1 : 2 electrolytes. The IR spectra confirmed the disappearances of both coordinated borohydride and acetonitrile. The observed bands are essentially ascribable to the stretching of coordinated N- and P-donor ligands and to the BF_4 counterion (ν_{BF_4} 1150–950 cm^{-1}).[64]

The high-frequency region of the ^1H NMR spectra shows, besides the signals related to aromatic phosphines and pyridine, pyrimidine or phenoxytriazine substituents, a set of

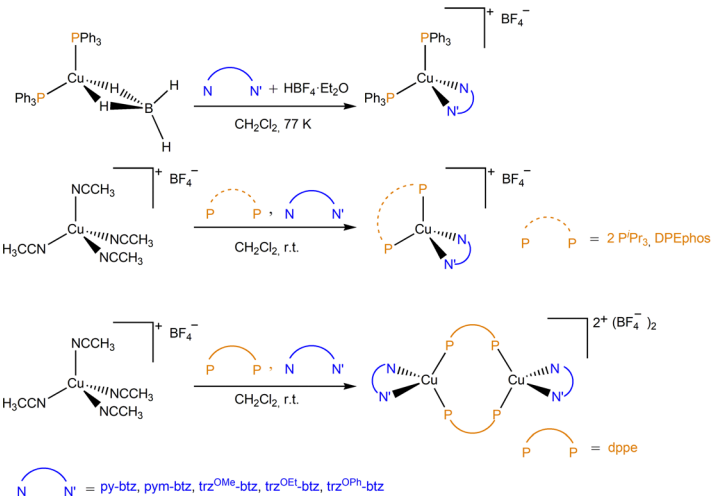

	PPh_3	P^iPr_3	dppe	DPEphos
py-btz	**1a** (90%)	**1b** (75%)	**1c** (79%)	**1d** (90%)
pym-btz	**2a** (88%)	**2b** (75%)	**2c** (76%)	**2d** (87%)
trz^{OMe}-btz	**3a** (85%)	**3b** (78%)	**3c** (78%)	**3d** (82%)
trz^{OEt}-btz	**4a** (91%)	**4b** (81%)	**4c** (80%)	**4d** (89%)
trz^{OPh}-btz	**5a** (78%)		**5c** (83%)	**5d** (83%)

Scheme 2 Synthesis of Cu(I) complexes. Yields in brackets.

resonances for the benzotriazole heterocycle. In the aliphatic region, the P-bonded $-CH(CH_3)_2$ or $-CH_2CH_2-$ resonances are detectable for the **1b–4b** and **1c–5c** complexes. Two distinct groups of resonances for the O-bonded substituents were observed at low temperatures for selected trz^{OMe}-btz and trz^{OEt}-btz complexes, depending upon the choice of the phosphine and the bulk of the alkoxy groups. In particular, two separate –OR groups were detected for the PPh_3 and dppe derivatives **3a**, **3c** and **4a**, **4c**. On the other hand, in the ^1H NMR spectra of the P^iPr_3 complexes **3b** and **4b**, only one set of resonances is present. Finally, the trz^{OMe}-btz DPEphos complex **3d** shows only one singlet for the two –OMe groups at 243 K, while two distinct –OEt fragments are recognizable in the ^1H NMR spectrum of the related trz^{OEt}-btz species **4d** under the same experimental conditions. The effects of coordination on the chemical equivalence are present also for some pym-btz derivatives, **2c** and **2d** in particular. The solutions of the complexes in $CDCl_3$ maintained the same ^1H and $^{31}P\{^1H\}$ NMR resonances after more than two weeks, so arrangement processes of fast ligands can be excluded.

Crystals suitable for X-ray diffraction were isolated from CH_2Cl_2/Et_2O (**1a**, **2b**, **2c**, **3b** and **5d**), CH_2Cl_2/EtOH (**2a**, **1d**) and from the slow evaporation of CH_2Cl_2 solutions (**4d**).

Crystal data and structure refinement of complexes **1a** and **2a** are reported in Table S2 (ESI†). The structure of $[\mathbf{1a}]^+$ is shown in Fig. 1 (see Fig. S31, ESI† for the ellipsoid plot of both the cations). The py-btz and pym-btz ligands behave as chelate N-donors and the Cu(I) coordination sphere is completed by two PPh_3. Although the complexes differ only for one nitrogen atom, they exhibit important differences in the packing, and consequently, the molecules are not superimposable (see Fig. S32, ESI†). The reason may rely on the conformation of the N-donor ligand and the supramolecular network, in part generated in the case of **2a** by the π,π-stacking between the pyrimidine ring and the benzene fragment of a neighbour btz ring with symmetry operation $1-x$, $1-y$, and $2-z$ (see Fig. S33, ESI†). The distance between the centroids of these planes is

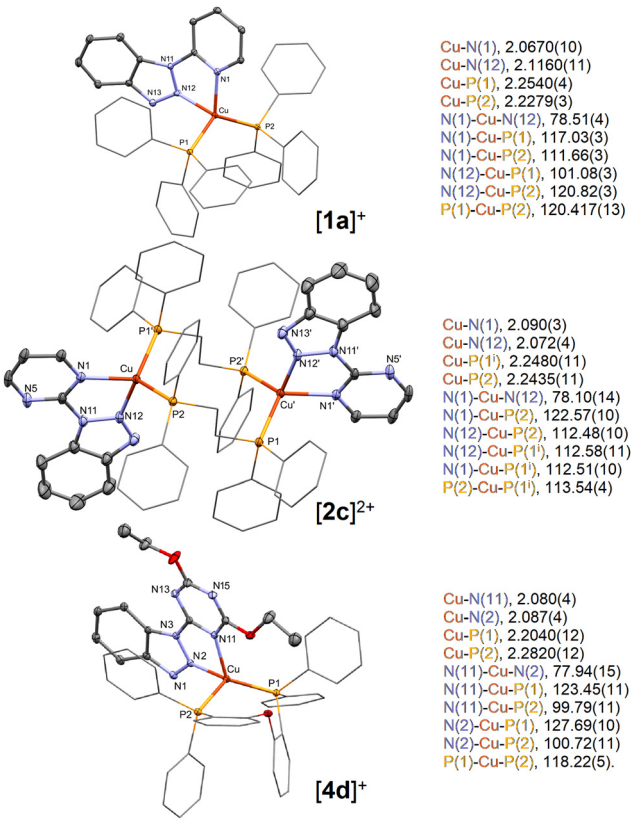

Fig. 1 Ellipsoid plot of the cations $[\mathbf{1a}]^+$, $[\mathbf{2c}]^{2+}$ and $[\mathbf{4d}]^+$. Hydrogen atoms are omitted for clarity.

3.6026(16) Å, with a slippage of 1.344 Å, and the dihedral angle between them is 1.89(13)°. A comparable π,π-stacking interaction does not exist in the crystal structure of **1a**.

Crystal data and structure refinement for the complexes **2b**, **1d**, **2c**, **3b**, **4d** and **5d** are reported in Tables S3 and S4 (ESI†). The structures of $[\mathbf{2c}]^{2+}$ and $[\mathbf{4d}]^+$ are shown in Fig. 3. Ellipsoid plots of all the complexes are reported in Fig. S34 (ESI†).

Selected bond distances and angles are set out in Tables S5–S8 (ESI†).

The Cu–P bond lengths depend upon the phosphine, being shorter for PPh_3 and DPEphos derivatives and longer for P^iPr_3 complexes. The Cu–N bond lengths are also influenced by the choice of the phosphine, since longer Cu–P bonds correspond to shorter Cu–N bonds. Noticeable differences can be detected by comparing the angles in the environment of Cu atoms. Only in the P^iPr_3 complexes **2b** and **3b**, the P–Cu–P angle is the biggest, with values of 132.95(5)° and 130.51(1)°, respectively, and represents the main source of distortion from tetrahedral geometry. In the case of the cations $[\mathbf{1d}]^+$, $[\mathbf{4d}]^+$ and $[\mathbf{5d}]^+$ several N–Cu–P angles are more obtuse than the P–Cu–P angle, probably because of the bidentate character of the DPEphos ligand (see Tables S6 and S8, ESI†). The same situation was previously observed in similar compounds.[65–68] The P–Cu–P angle is also the most important difference between compounds **2a** and **2b**, as detectable in the superimposition reported in Fig. S35 (ESI†). Although the value for **2b** is surprisingly large, it is far from the angle of 149.02(6)° found in a similar compound having 2-(pyridin-2-yl)quinoxaline as a ligand.[47] Moreover, as previously observed in complex **1a**, also for **2b**, π,π-stacking interaction is not observed, probably because of the steric hindrance of the isopropyl groups.

In complex **3b**, trz^{OMe}-btz maintains the same conformation and planarity observed in the free ligand. The root-mean square deviation from the best-fitted plane (calculated for 15 atoms) is equal to 0.057 Å, while in the free ligand, it was 0.070 or 0.029 Å. The –OMe carbons are instead one 0.282(2) Å below and the other one 0.251(2) Å above the plane. Cu atoms lie mainly in the plane, being displaced by only 0.024(1) Å. As for trz^{OMe}-btz, the aliphatic substituents of trz^{OEt}-btz maintain the same disposition in the corresponding complex **4d**, *i.e.* one in *syn* and the other one in *anti*. The aromatic groups of trz^{OPh}-btz in **5d** are instead situated both in *syn*, in opposition to what was found in the free ligand, where they were both in *anti*. This outcome is understandable for one of the phenoxy-groups, otherwise, N(11) would be too sterically hindered to act as a ligand. The superimposition of complex **5d** with the free ligand is reported in Fig. S36 (ESI†). The planarity of the N-donors is reduced by coordination, in such a way that the root-mean-square deviation for the 15 atoms forming the central body is 0.1149 Å for **4d** and 0.0834 Å for **5d** (0.0062 Å in the free species). In complex **5d**, the dihedral angle between this plane and each phenyl ring is 62.10(5) and 64.35(4)°. Instead, Cu(I) atom is out of the plane, being deviated by 0.344(3) Å and 0.087(1) Å respectively, in **4d** and **5d**. One phenoxy oxygen atom is deviated up to 0.373(1) Å from the plane. In other words, the five-membered metallacycle is puckered into an envelope conformation with coordinates $Q(2) = 0.104(4)$ Å and $\phi(2) = 4(2)°$ for **4d**, and $Q(2) = 0.0955(11)$ Å and $\phi(2) = 151.4(7)°$ for **5d**.[69]

The two bidentate phosphines considered afforded different results. DPEphos behaves as a chelating P-donor, as observed for the majority of the complexes reported in CCDC,[70] while dppe acts as a bridging ligand. The P···P distance in free DPEphos is between 4.876 Å and 4.881 Å.[71,72] Once coordinated to Cu(I), such a distance is reduced to values between 3.7054(5) (**5d**) and 3.8755(8) Å (**1d**). For comparison, in the tricoordinated cation $[Cu(DPEphos)_2]^+$, one of the phosphorus atoms is not coordinated and the P···P distance increases up to 5.08 Å, while for the chelating DPEphos, this value is around 3.8 Å.[73] Similar values were found also in other complexes with this κ^2-ligand.[39,48–53] On the other hand, the distance P···P in free dppe is between 4.437 Å and 4.463 Å,[74,75] that is maintained also in the corresponding complex **2c**, where it is equal to 4.445(2) Å.

The environment around the Cu(I) ions could be described as tetrahedral in all the complexes, but it is highly distorted. Continuous Shape Measures calculation [SHAPE V2.1][76] gives the vacant trigonal bipyramid as the best geometry approximation for these compounds (C_{3v} symmetry, axial vacant). The output data for all the complexes are collected in Table S9 (ESI†) together with the parameters used to evaluate the distortion of a tetrahedron.[77–80] The values range from 0.77 to 0.88 (τ_4) or from 0.75 to 0.85 (τ_4'), suggesting a large deviation from the perfect tetrahedral geometry. It is worth noting that for both the parameters, 1.0 corresponds to the tetrahedron, 0.0 to the square planar and 0.85 to the trigonal prism. The cation of compound **5d** is best described as a vacant trigonal bipyramid, being τ_4 and τ_4' equal to 0.85.

Electrochemical, absorption and emission measurements

Electrochemical measurements on **1a** and **4d** and on the free py-btz and trz^{OEt}-btz ligands show irreversible processes related to the oxidation of the $\{CuP_2\}$ fragment starting around 0.75 V *vs.* Fc/Fc^+ (Fig. 2). Several other oxidation processes occur at higher potential, closely comparable to those observed for the free N-donor ligands. The first reduction process is observable for potentials lower than −1.75 V in the case of **1a** and lower than −1.65 V for **4d**. The reduction processes of the free ligands start at lower potentials, in particular in the case of py-btz. This outcome can be ascribed to the σ-donation of electron density to the Cu(I) centre, which makes the N-donor heterocycles more electron deficient and therefore more oxidant. The reduction processes are irreversible in all the cases. The potential gap between first oxidation and first reduction is in the 2.6–3.1 V range for **1a**, while it is slightly lower for **4d** (2.4–2.8 V range).

The complexes are characterized by absorptions for wavelengths below 500 nm in diluted CH_2Cl_2 solutions. The superimposition of the UV-vis spectra of complexes **2a–2d** is reported in Fig. 3 and for all the other complexes in Fig. S37 (ESI†). The maximum molar extinction coefficients are comprised between 30 000 and 60 000 M^{-1} cm^{-1}. The tails in the visible range account for the yellow colour observed for concentrated solutions and powder samples. The comparison with the free ligands allows us to point out that the absorption spectra are almost in part related to the $\pi^* \leftarrow \pi$ transitions of the aromatic fragments.

In the case of aromatic phosphine derivatives, it is also possible to notice a band tentatively attributed to MLCT transitions around 400 nm. The same band is present, but with a

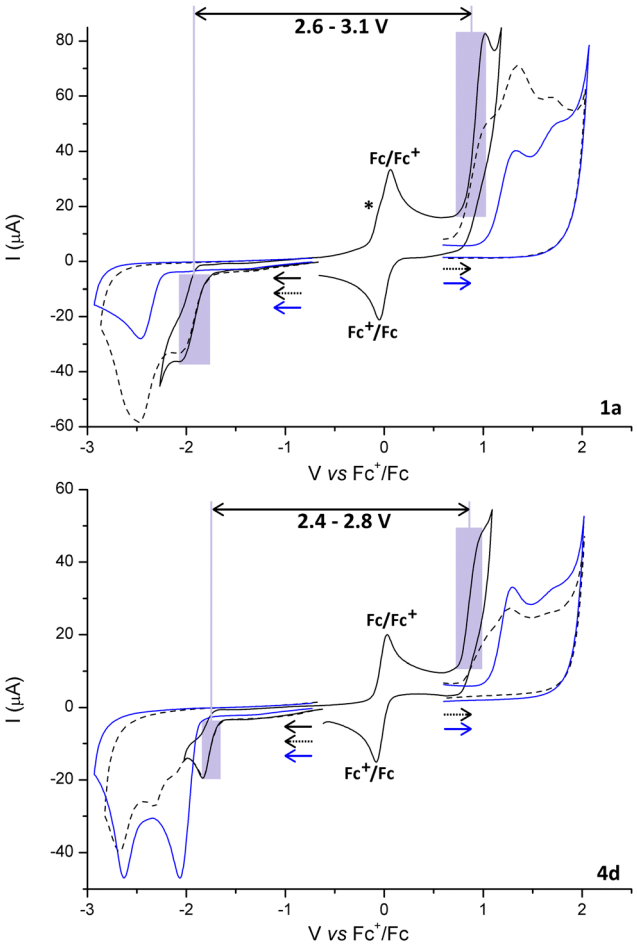

Fig. 2 Cyclic voltammetries of **1a** and **4d** (from the first reduction to the first oxidation, continuous black lines; extended cathodic and anodic scans, dashed black lines) and of py-btz and trz^{OEt}-btz (continuous blue lines). Glassy carbon electrode, acetone/$LiClO_4$, 500 mV s^{-1}, ferrocene as internal standard, r.t., Ar atmosphere. The * symbol highlights the reverse oxidation process related to the first reduction of **1a**.

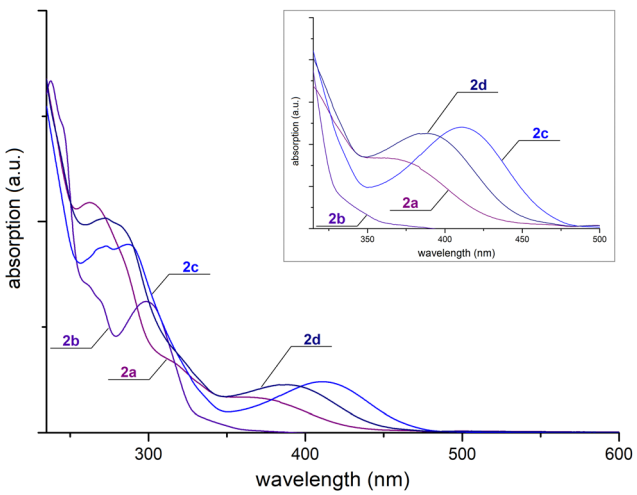

Fig. 3 Absorption spectra of complexes 10^{-5} M in CH_2Cl_2 (**2a**, purple line; **2b**, violet line; **2c**, navy blue line; **2d**, blue line).

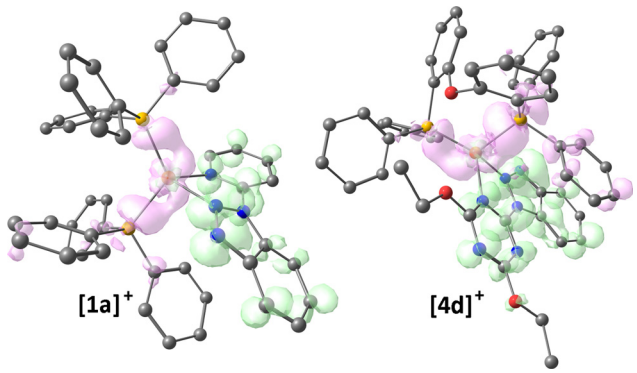

Fig. 4 DFT-optimized structures of [**1a**]$^+$ and [**4d**]$^+$ (ground singlet states) with hole (pink) and electron (green) distributions related to the lowest energy singlet–singlet transitions (surface isovalue = 0.003 a.u.). Colour map: Cu, orange; P, yellowish orange; O, red; N, blue; C; grey. Hydrogen atoms are omitted for clarity.

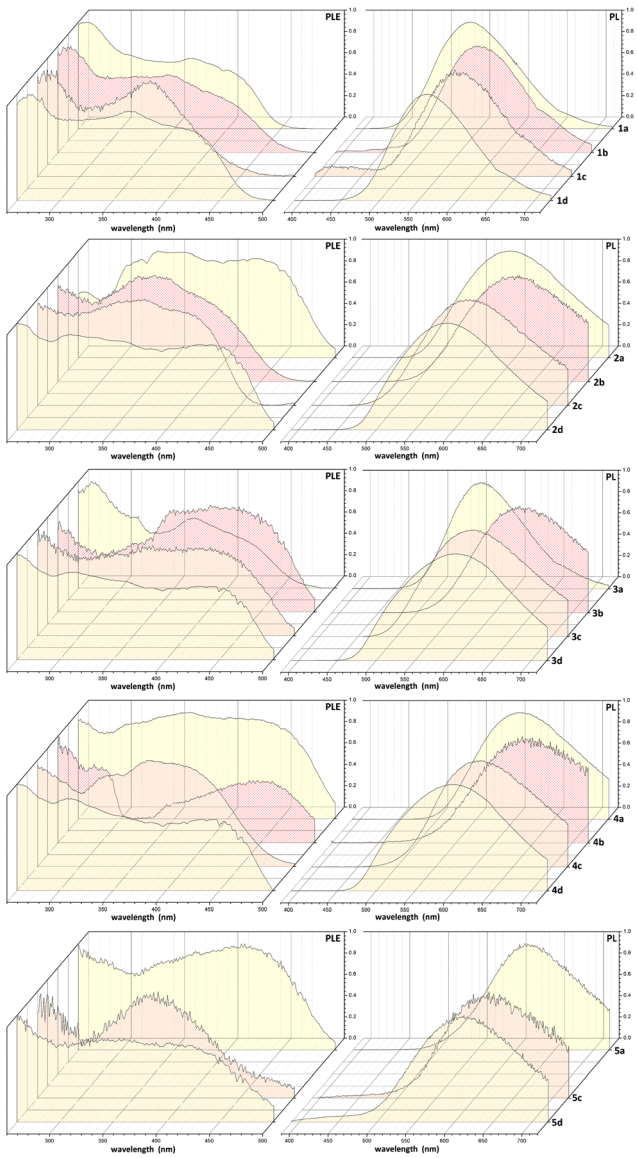

Fig. 5 PL and PLE spectra of the complexes (solid state, r.t.). See Table 1 for experimental details.

Table 1 Photophysical data of the complexes

	UV-vis[a] nm	PL (FWHM)[b] nm (cm^{-1})	PLE[c] nm	Stokes shift[d] cm^{-1}	τ^e μs	Φ^f (%)
1a	<430, 262 (ε = 44 500 M^{-1} cm^{-1}), 270 (sh), 285 (sh), 307 (sh), 365 (sh)	538 (FWHM = 4100)	<440	8800	164	26
1b	<350, 238, 247 (sh), 272 (ε = 59 900 M^{-1} cm^{-1}), 282 (sh)	575 (FWHM = 3800)	<470	—	34	10
1c	<475, 266 (sh), 272, 289 (ε = 47 200 M^{-1} cm^{-1}), 404	580 (FWHM = 3800)	<450	7500	47	4
1d	<475, 264 (sh), 272 (sh), 288 (ε = 31 200 M^{-1} cm^{-1}), 382	561 (FWHM = 3700)	<470	8400	14	13
2a	<450, 263 (ε = 21 800 M^{-1} cm^{-1}), 310 (sh), 370 (sh)	558 (FWHM = 4100)	<500	9100	20	35
2b	<380, 238 (ε = 33 300 M^{-1} cm^{-1}), 245 (sh), 261 (sh), 268 (sh), 298	588 (FWHM = 3600)	<475	—	23	7
2c	<475, 267 (sh), 273, 287 (ε = 17 800 M^{-1} cm^{-1}), 412	561 (FWHM = 3500)	<460	6500	23	6
2d	<475, 273 (ε = 20 300 M^{-1} cm^{-1}), 282 (sh), 388	557 (FWHM = 4200)	<500	7800	37	36
3a	<450, 260 (ε = 10 800 M^{-1} cm^{-1}), 387	557 (FWHM = 3600)	<460	7900	32	7
3b	<350, 237 (ε = 33 400 M^{-1} cm^{-1}), 263 (sh), 270 (sh), 299	637 (FWHM = 4000)	<500	—	21	2
3c	<500, 267 (sh), 273, 290 (ε = 26 700 M^{-1} cm^{-1}), 433	598 (FWHM = 4500)	<500	6400	11	6
3d	<490, 265 (sh), 273 (ε = 34 300 M^{-1} cm^{-1}), 407	604 (FWHM = 5000)	<500	8000	65	6
4a	<450, 259 (ε = 18 800 M^{-1} cm^{-1}), 314 (sh), 380	577 (FWHM = 3400)	<520	9000	5	17
4b	<350, 261, 270 (sh), 297 (ε = 15 300 M^{-1} cm^{-1}), 328 (sh)	600 (FWHM = 3600)	<515	—	43	14
4c	<500, 267 (ε = 25 400 M^{-1} cm^{-1}), 272 (sh), 289, 429	578 (FWHM = 3300)	<475	6600	11	17
4d	<460, 265 (sh), 272 (ε = 30 600 M^{-1} cm^{-1}), 404	550 (FWHM = 4200)	<475	6600	43	92
5a	<470, 259 (ε = 40 000 M^{-1} cm^{-1}), 319 (sh), 390	615 (FWHM = 3700)	<500	9400	23	2
5c	<530, 268, 273, 293 (ε = 25 600 M^{-1} cm^{-1}), 442	571 (FWHM = 4800)	<470	5100	14	3
5d	<500, 274 (ε = 39 000 M^{-1} cm^{-1}), 318 (sh), 415	598 (FWHM = 4000)	<510	7400	4	7

[a] CH_2Cl_2 solution, 298 K. [b] Powder samples, r.t., $\lambda_{excitation}$ = 350 nm (**1b**, **1c**, **1d**, **2a**, **2b**, **2c**, **3a**, **3d**, **4a**, **4b**, **4c**, **4d**, **5a**); 365 nm (**1d**, **5c**, **5d**); 375 nm (**1a**); 415 nm (**3b**, **3c**). [c] Powder samples, r.t., $\lambda_{emission}$ = 525 nm (**4d**); 535 nm (**1a**); 555 nm (**3a**); 570 nm (**1c**, **1d**, **2a**, **2c**, **2d**); 575 nm (**1b**, **4a**, **4c**); 590 nm (**2b**, **3c**); 610 nm (**4b**); 620 nm (**5a**); 630 (**3b**, **3d**, **5c**, **5d**). [d] Not determined for the P^iPr_3 derivatives because of the difficult assignment of the maximum of MLCT absorptions. [e] Powder samples, r.t., $\lambda_{excitation}$ = 290 nm (**1a**, **1b**, **1c**, **1d**, **3a**, **4a**, **4b**, **4c**, **4d**, **5c**, **5d**); 445 nm (**2a**, **2b**, **2d**, **3b**, **3c**, **3d**, **5a**). [f] Powder samples, r.t., $\lambda_{excitation}$ = 365 nm.

much lower extinction coefficient, also for the P^iPr_3 complexes **1b–4b**. The onsets of the lowest energy absorptions of **1a**, about 400 nm, and of **4d**, about 450 nm, are perfectly in line with the potential gaps between the first oxidation and the first reduction of the complexes, supporting the MLCT assignment.

DFT calculations on $[\mathbf{1a}]^+$ and $[\mathbf{4d}]^+$ as representative compounds confirmed the MLCT nature of the lowest energy absorption. The computed ground-state stationary points are in good agreement with the X-ray data (RMSD of 0.353 Å and 0.480 Å for $[\mathbf{1a}]^+$ and $[\mathbf{4d}]^+$, respectively) and the computed wavelength of the lowest energy singlet ← singlet transitions are in line with the absorption spectra (341 nm for $[\mathbf{1a}]^+$ and 376 nm for $[\mathbf{4d}]^+$). The hole and electron distributions associated with the singlet–singlet transition, depicted in Fig. 4, clearly indicate that the electron moves from an occupied orbital centred on the $\{CuP_2\}$ fragment to an unoccupied π* orbital localized on the N-donor heterocycle. In both cases, the absorption is related to a transition involving the frontier orbitals, and the computed distance between the centres of hole and electron distributions is around 2.9 Å.

Excitation of powder samples with near-UV and violet light affords emissions from yellow to reddish-orange centred between 538 and 637 nm. The luminescence is not maintained in the solution. The normalized PL and PLE spectra are shown in Fig. 5. On comparing complexes with the same N-donor chelate, the emission maxima fall at longer wavelengths when P^iPr_3 is used as a P-donor ligand. The choice of the N-donor ligands also influences the emission maximum, with longer wavelengths generally observed for the trz^{OPh}-btz derivatives. Photophysical data for all the complexes are summarized in Table 1.

Despite the roughly comparable PL and PLE spectra, the photoluminescence quantum yield values (Φ) are markedly different. Table 1 indicates that weaker emission was in general observed for the mononuclear P^iPr_3 complexes and the dinuclear dppe derivatives. The flexibility of the isopropyl substituents and of the ethylene bridges probably favours non-radiative decay routes. Moreover, in the P^iPr_3 derivatives, there is no possibility of extra-stabilization offered by π–π stacking with the N-donor chelates, differently from the other complexes here considered.

For what concerns the N-donor ligands, the worst results were achieved using trz^{OPh}-btz and trz^{OMe}-btz. On the other hand, higher Φ values were surprisingly measured using the comparable trz^{OEt}-btz ligand. The quantum yield values do not however show any evident trend related to the choice of the P- or N-donor ligands. For instance, higher Φ was obtained with py-btz in combination with PPh_3 (**1a**) with respect to DPEphos (**1d**), while the related pym-btz complex **2a** and **2d** have very similar quantum yields. The measured Φ of the trz^{OEt}-btz PPh_3 derivative **4a** is 17%, while the value increases up to the astonishing value of 92% by replacing the two PPh_3 ligands with DPEphos (**4d**). It is to conclude that the combined electronic and steric features of the coordinated ligands play a hardly predictable role in the stabilization of ground and excited states. As an example, for what concerns the ground state geometry the methoxy-substituted complex **3d** revealed fluxional behaviour in solution, differently from the more rigid ethoxy-substituted derivative **4d** under the same experimental conditions.

The Stokes shifts (not reported for the P^iPr_3 derivatives because of the difficult assignment of the maximum of MLCT absorptions) are comprised between 5100 and 9400 cm^{-1}. The highest values are generally related to the PPh_3 complexes, while the lowest is to the dppe derivatives. The high Stokes shift range and the wide emissions (FWHM between 3500 and 5000 cm^{-1})

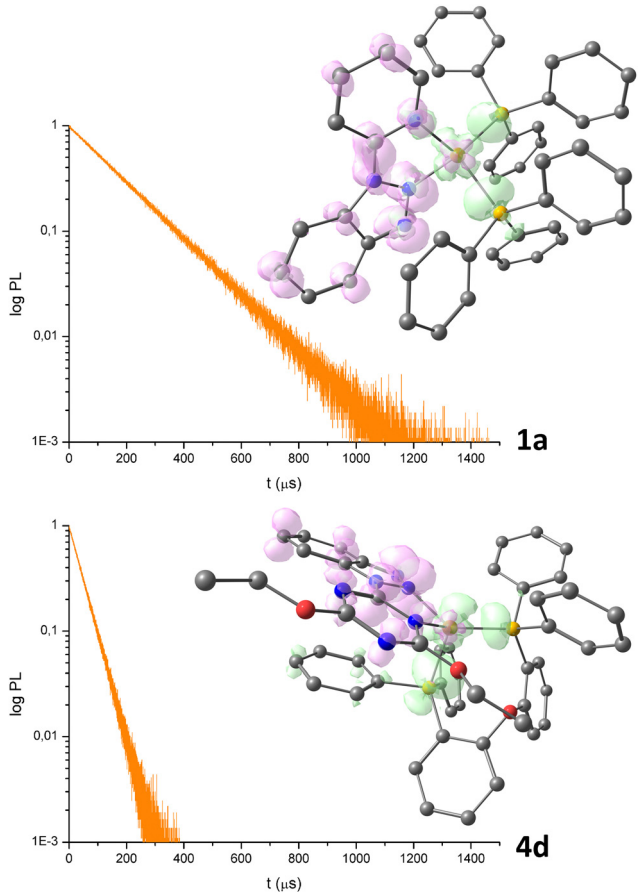

Fig. 6 Luminescence decay curves of **1a** and **4d** (see Table 1 for experimental details) and DFT-optimized structures of $[\mathbf{1a}]^+$ and $[\mathbf{4d}]^+$ (triplet states) with hole (pink) and electron (green) distributions related to the lowest energy triplet-singlet transitions (surface isovalue = 0.003 a.u.). Colour map: Cu, orange; P, yellowish orange; O, red; N, blue; C; grey. Hydrogen atoms are omitted for clarity.

suggest that triplet excited states are involved in the luminescence. Such an outcome is confirmed by luminescent lifetime (τ) values in the microseconds range.

Table 1 reveals that lifetime values depend upon the Cu(I) coordination sphere, but there is no linear correlation with the photoluminescence quantum yields. For instance, the longest τ, 164 μs, is that of complex **1a**, having Φ equal to 26%, while for the most efficient **4d** complex, the τ value is 43 μs (see Fig. 6 for the luminescence decay curves).

The radiative (k_r) and non-radiative (k_{nr}) constants for **4d**, estimated on the basis of the equation $\Phi = k_r/(k_r + k_{nr}) = \tau\, k_r$ are $k_r = 2.1 \times 10^4\ s^{-1}$ and $k_{nr} = 1.8 \times 10^3\ s^{-1}$. For comparison, the same constants for **1a** are $k_r = 1.6 \times 10^3\ s^{-1}$ and $k_{nr} = 4.6 \times 10^3\ s^{-1}$.[21]

The computationally optimized structures of $[\mathbf{1a}]^+$ and $[\mathbf{4d}]+$ in triplet state (Fig. 6) are comparable to the relative singlet ground states (RMSD of 0.563 Å for $[\mathbf{1a}]^+$ and 0.525 Å for $[\mathbf{4d}]+$). The analysis of the hole and electron distributions related to the lowest energy triplet-singlet transitions gives a picture in line with the previously discussed MLCT absorptions, with the electron moving from a π* orbital localized on the N-donor heterocycle to the $\{CuP_2\}$ fragment.

Table 2 Computed energy gaps between ^{1}MLCT and ^{3}MLCT states at the singlet and triplet geometries of $[\mathbf{1a}]^+$ and $[\mathbf{4d}]^+$

	$\Delta E(^1\text{MLCT}–^3\text{MLCT})$, cm^{-1}	
	Singlet geometry	Triplet geometry
$[\mathbf{1a}]^+$	4360	4000
$[\mathbf{4d}]^+$	3130	2750

On the basis of experimental and computational outcomes, the emissions are therefore attributed to ^{3}MLCT transitions. The computed energy gaps between singlet and triplet MLCT states, collected in Table 2, are all in the thousands of cm^{-1} range and do not support the possibility of the TADF mechanism, usually invoked for energy gaps below 1000 cm^{-1}.[22]

Conclusions

Cu(I) complexes with π-delocalized N-donor ligands represent a viable alternative to heavy transition metal derivatives for advanced technology since their photophysical properties can be largely tuned by modifying the coordinated ligands. In this context, here we reported the successful synthesis and characterization of several photoluminescent complexes with N-donor chelates containing the btz fragment bonded to a six-membered heterocycle. Noticeable luminescence in the yellow-reddish orange range is associated with excitation in the near-UV and violet transition, with processes related to MLCT transitions and intersystem crossing. The data provided highlight strong and quite unexpected dependence of the emission features upon the introduction of small variations in the N-donor chelate, in particular the photoluminescence quantum yield. Moreover, the best performances are achieved only when the bidentate heterocycles are combined with the proper phosphine in the Cu(I) coordination sphere. The cationic mononuclear complex with coordinated trz^{OEt}-btz and DPEphos appears to be particularly appropriate for advanced devices thanks to its high quantum yield, wide excitation range, and lifetime in the microseconds range. The inexpensive benzotriazole heterocycle confirms to be a well-suited building block for the preparation of luminescent Cu(I) derivatives, and the strong variability of the results here provided suggests that further improvements are possible.

Experimental section

Materials and methods

Commercial solvents (Merck) were purified following reported procedures in order to be used inside the glove-box.[81] All the other reagents were Sigma Aldrich products used as received. $[Cu(\kappa^2\text{-}BH_4)(PPh_3)_2]$ and $[Cu(NCCH_3)_4][BF_4]$ were obtained from reported syntheses.[82,83] 2-chloro-4,6-dimethoxy-1,3,5-triazine (CDMT), 2-chloro-4,6-ethoxy-1,3,5-triazine (CDET)

and 2-chloro-4,6-phenoxy-1,3,5-triazine (CDPhT) were prepared following previously described methods.[84,85]

The syntheses of the complexes starting from $[Cu(NCCH_3)_4][BF_4]$ were carried out in an inert atmosphere in a glove-box (MBraun Labstar with MB 10 G gas purifier) filled with N_2 and equipped for inorganic syntheses. The reactions starting from $[Cu(\kappa^2\text{-}BH_4)(PPh_3)_2]$ were carried out using standard Schlenk techniques.

Elemental analyses (C, H, N) were carried out using an Elementar Unicube micro analyzer. Conductivity measurements in acetone were performed using a Radiometer Copenhagen CDM83 instrument. Melting point measurements were carried out using a modified Falc 360 D apparatus equipped with a video recording device. IR spectra (KBr pellets) were collected in the range of 4000–400 cm^{-1} using a PerkinElmer Spectrum One spectrophotometer. Heteronuclear magnetic resonance (NMR) spectra were recorded at variable temperatures employing Bruker Avance 300 and Avance 400 instruments operating, respectively, at 300.13 MHz and 400.13 MHz of ^1H resonance. ^1H and $^{13}C\{^1H\}$ NMR spectra are referred to as the partially non-deuterated fraction of the solvent, itself quoted to tetramethylsilane. $^{31}P\{^1H\}$ NMR spectra are referred to as 85% H_3PO_4 in water. Cyclic voltammetry measurements were performed using an eDAQ ET014-199 instrument in acetone containing 0.1 M $LiClO_4$. The solvent was purified following common techniques[81] and all the measurements were carried out under argon at room temperature. The working electrode was a 1 mm glassy carbon disk, while the auxiliary electrode was a Pt-coated titanium rod. The electrodes were provided by eDAQ. Ferrocene was introduced as an internal standard and a Pt wire was used as a pseudo-reference electrode.

Crystal structure determination

Crystallographic data were collected at CACTI (University of Vigo) at 100 K (CryoStream 800) using a Bruker D8 Venture Photon II CMOS detector with Mo-Kα radiation (λ = 0.71073 Å) generated by an Incoatec Microfocus Source IμS. The software APEX3 was used for collecting frames of data, indexing reflections, and the determination of lattice parameters, SAINT for integration of intensity of reflections, and SADABS for scaling and empirical absorption correction.[86] The crystallographic treatment was performed with the Oscail program,[87] solved using the SHELXT program.[88] The structure was subsequently refined by a full-matrix least-squares based on F^2 using the SHELXL program.[89] The reflections affected by the beam stop were systematically removed from the final refinement. Non-hydrogen atoms were refined with anisotropic displacement parameters. Hydrogen atoms were included in idealized positions and refined with isotropic displacement parameters. In a number of cases, special procedures were used. In the case of the trz^{OMe}-btz crystal, twinning was solved by means of the twin instruction on the classical SHELXL process. Instead, crystal twinning for trz^{OPh}-btz was corrected by the TwinRotMat subroutine in PLATON, and the structure was refined as a 2-component perfect twin.[90] Further details concerning crystal data and structural refinement are given in Table S1 (ESI†). In the case of the compounds **1a** and **2a** disordered solvent molecules, probably MeOH in the former and EtOH in the latter, were found in the final density map, and their contribution was eliminated by using the SQUEEZE procedure on PLATON.[90] A disorder on the tetrafluoroborate anion is also present in complex **2a**, which was not resolved. Crystal data and structural refinement for complexes **1a** and **2a** are collected in Table S2 (ESI†). It should be also noted that compound **1d** crystallizes in the monoclinic *C*2/*c* space group with two molecules in the asymmetric unit. One of them is characterized by some disorder, with an occupancy factor of 0.57(1) : 0.43(1). For the dimeric compound **2c**, the SQUEEZE procedure was also used. Once again, the tetrafluoroborate anion appeared so disordered that the anisotropic displacement parameters of the fluorine atoms were fixed by using the *sadi* instruction on SHELXL. Crystal data and structural refinement for complexes **2b**, **2c** and **1d** are given in Table S3 (ESI†). In the case of compound **4d**, one of the ethoxy groups and the tetrafluoroborate anion resulted to be so disordered that the anisotropic displacement parameters of some atoms were fixed by using the *sadi* and *eadp* instructions on SHELXL. The quality of the crystal data did not allow to fix all the problems, and important residual electronic densities remained after the last refinement. They are probably part of the disordered molecule, not modelled. Crystal data and structural refinement for complexes **3b**, **4d** and **5d** are given in Table S4 (ESI†). PLATON (version 60720) was used to obtain some geometrical parameters from the cif files.[90]

Photophysical measurements

Absorption spectra in CH_2Cl_2 solutions were collected using a PerkinElmer Lambda 40 spectrophotometer. Photoluminescence measurements on solid samples were carried out using air-tight quartz sample holders, filled in glove-box to avoid interactions of the complexes with moisture. Photoluminescence emission (PL) and excitation (PLE) measurements were carried out at room temperature on solid samples using a Horiba Jobin Yvon Fluorolog-3 spectrofluorometer. A continuous-wave xenon arc lamp was used as a source selecting the excitation wavelength using a double Czerny–Turner monochromator. A single grating monochromator coupled to a photomultiplier tube was used as a detection system for optical emission measurements. Excitation and emission spectra were corrected for the instrumental functions. Time-resolved analyses were performed in multi-channel scaling modality (MCS) by using a pulsed UV-led source (Horiba SpectraLEDs) centred at 290 or 445 nm. Photoluminescence quantum yield Φ of the complexes (solid state, r.t.) was measured using an OceanOptics HR4000CG UV-NIR detector, fiber-coupled to an integrating sphere connected to an OceanOptics LED source centred at 365 nm. The values were reported as the average of three measurements.

Computational details

Ground and excited state structures of the complexes $[\mathbf{1a}]^+$ and $[\mathbf{4d}]^+$ were optimized using the global-hybrid meta-NGA

functional MN15 DFT functional and the Ahlrichs and Weigend's def2 split-valence polarized basis set.[91,92] The C-PCM implicit solvation model was added to MN15 calculations, considering CH_2Cl_2 as a continuum medium.[93,94] The relative energies of the excited states were obtained by carrying out TD-DFT (time-dependent DFT) calculations at the same theoretical level, starting from singlet and triplet state geometries.[95] Calculations were carried out using Gaussian 16 and the output files were analysed with Multiwfn, version 3.5.[96,97] Cartesian coordinates of the DFT-optimized structures are provided in a separated .xyz file.

Synthesis and characterization of the ligands

The syntheses of 1-(pyridine-2-yl)benzotriazole (py-btz) and 1-(pyrimidin-2-yl)benzotriazole (pym-btz) were carried out following methods previously reported by Katritzky *et al.*[61,62]

Synthesis of 1-(4,6-alkoxy-1,3,5-triazin-2-yl)benzotriazole (trz^{OR}-btz, R = Me, Et, Ph)

The ligands were prepared by reacting 15.0 mmol of 4,6-alkoxy-substituted 2-chloro-triazine and 3.574 g of benzotriazole (30.0 mmol) in 20 mL of dry CH_2Cl_2 for CDMT or toluene for CDET and CDPhT. To prepare trz^{OMe}-btz, the reaction mixture was stirred at room temperature overnight and then heated to reflux for 3 hours. For trz^{OEt}-btz and trz^{OPh}-btz, the reaction mixture was refluxed for 18 hours in an N_2 atmosphere. After cooling down to room temperature, trz^{OMe}-btz and trz^{OPh}-btz were extracted with CH_2Cl_2, while trz^{OEt}-btz was treated with Et_2O. The so-obtained mixture was washed with 2 × 50 mL of cold NaOH 10% and 2 × 50 mL of water. The organic fractions were collected and dried with Na_2SO_4. The solvents were evaporated under reduced pressure to afford the products as white solids. Yield >80% in all the cases.

Characterization of 1-(4,6-methoxy-1,3,5-triazin-2-yl)benzotriazole (trz^{OMe}-btz). Anal. calcd for $C_{11}H_{10}N_6O_2$ (258.54 g mol^{-1}, %): C, 51.16; H, 3.90; N, 32.54. Found (%): C, 50.96; H, 4.10; N, 32.41. Mp: 181 °C. ^1H NMR ($CDCl_3$, 298 K) δ 8.58 (d, 1H, $^3J_{HH}$ = 8.4 Hz, btz), 8.20 (d, 1H, $^3J_{HH}$ = 8.3 Hz, btz), 7.70 (dd, 1H, $^3J_{HH}$ = 8.4 Hz, $^3J_{HH}$ = 7.1 Hz, btz), 7.54 (dd, 1H, $^3J_{HH}$ = 8.3 Hz, $^3J_{HH}$ = 7.1 Hz, btz), 4.25 (s, 6H, $-CH_3$). $^{13}C\{^1H\}$ NMR ($CDCl_3$, 298 K) δ 173.42 (*ipso*-trz), 146.85 (*ipso*-trz), 140.56 (*ipso*-btz), 131.71 (*ipso*-btz), 129.91 (btz), 125.76 (btz), 120.56 (btz), 115.10 (btz), 56.04 ($-CH_3$). IR (KBr, cm^{-1}): 3120–3020 m/w (aromatic ν_{C-H}), 2960–2850 m (ν_{C-H}), 1610–1540 m (aromatic ν_{C-C} and ν_{C-N}). UV-vis (CH_2Cl_2, 298 K, nm) < 340, 241 (max), 262 (sh), 271 (sh), 304 (sh).

Characterization of 1-(4,6-ethoxy-1,3,5-triazin-2-yl)benzotriazole (trz^{OEt}-btz). Anal. calcd for $C_{13}H_{14}N_6O_2$ (286.30 g mol^{-1}, %): C, 54.54; H, 4.93; N, 29.36. Found (%): C, 54.32; H, 4.95; N, 29.24. Mp: 120 °C. ^1H NMR ($CDCl_3$, 298 K) δ 8.57 (d, 1H, $^3J_{HH}$ = 8.4 Hz, btz), 8.19 (d, 1H, $^3J_{HH}$ = 8.7 Hz, btz), 7.69 (t, 1H, $^3J_{HH}$ = 7.2 Hz, btz), 7.53 (t, 1H, $^3J_{HH}$ = 7.8 Hz, btz), 4.67 (q, 4H, $^3J_{HH}$ = 7.1 Hz, $-CH_2$), 1.55 (t, 6H, $^3J_{HH}$ = 7.1 Hz, $-CH_3$). $^{13}C\{^1H\}$ NMR ($CDCl_3$, 298 K) δ 172.84 (*ipso*-trz), 164.66 (*ipso*-trz), 146.83 (*ipso*-btz), 131.70 (*ipso*-btz), 129.81 (btz), 125.66 (btz), 120.50 (btz), 115.08 (btz), 65.22 ($-CH_2$), 14.25 ($-CH_3$). IR (KBr, cm^{-1}): 3120–3000 m/w (aromatic ν_{C-H}), 2990–2880 m (ν_{C-H}), 1660–1600 m (aromatic ν_{C-C} and ν_{C-N}). UV-vis (CH_2Cl_2, 298 K, nm) < 340, 241 (max), 257 (sh), 270 (sh), 303 (sh).

Characterization of 1-(4,6-phenoxy-1,3,5-triazin-2-yl)benzotriazole (trz^{OPh}-btz). Anal. calcd for $C_{21}H_{14}N_6O_2$ (382.38 g mol^{-1}, %): C, 65.96; H, 3.69; N, 21.98. Found (%): C, 65.70; H, 3.70; N, 21.89. Mp: 210 °C. ^1H NMR ($CDCl_3$, 298 K) δ 8.13 (d, 1H, $^3J_{HH}$ = 8.0 Hz, btz), 7.69 (d, 1H, $^3J_{HH}$ = 8.1 Hz, btz), 7.51 (t, 4H, $^3J_{HH}$ = 7.9 Hz, Ph-H_{meta}), 7.45 (dd, 1H, $^3J_{HH}$ = 8.1 Hz, $^3J_{HH}$ = 7.1 Hz, btz), 7.40 (m, 1H, btz), 7.38 (m, 2H, Ph–H_{para}), 7.30 (m, 4H, Ph–H_{ortho}). $^{13}C\{^1H\}$ NMR ($CDCl_3$, 298 K) δ 173.54 (*ipso*-trz), 164.81 (*ipso*-trz), 151.71 (*ipso*-Ph), 146.72 (*ipso*-btz), 131.54 (*ipso*-btz), 129.82 (Ph–C_{meta}), 129.80 (btz), 126.51 (Ph–C_{para}), 125.79 (btz), 121.55 (Ph-C_{ortho}), 120.50 (btz), 115.00 (btz). IR (KBr, cm^{-1}): 3100–3015 m/w (aromatic ν_{C-H}), 1600–1550 m (aromatic ν_{C-C} and ν_{C-N}). UV-vis (CH_2Cl_2, 298 K, nm) < 340, 244 (max), 267 (sh), 308 (sh).

Synthesis and characterization of complexes 1a–5a

$HBF_4{\cdot}Et_2O$ (163 μL, 1.2 mmol) was added to 1.5 mmol of the proper N-donor ligand (py-btz, pym-btz, trz^{OMe}-btz, trz^{OEt}-btz or trz^{OPh}-btz) dissolved in 15 mL of CH_2Cl_2. The volatiles were evaporated under reduced pressure and 1.0 mmol (0.602 g) of $[Cu(\kappa^2\text{-}BH_4)(PPh_3)_2]$ was added. The reagents were kept in an inert atmosphere and cooled at 77 K with a liquid nitrogen bath. CH_2Cl_2 (20 mL) was then slowly added through a syringe and the reaction mixture was allowed to slowly warm up to room temperature. After stirring overnight, the solution was purified by filtration and CH_2Cl_2 was evaporated under reduced pressure. The addition of Et_2O (20 mL) caused the separation of a solid, that was filtered, washed with 5 mL of Et_2O and dried *in vacuo*. Yield > 75% in all the cases.

Characterization of $[Cu(py\text{-}btz)(PPh_3)_2][BF_4]$ (1a). Anal. calcd for $C_{47}H_{38}BCuF_4N_4P_2$ (871.15 g mol^{-1}, %): C, 64.80; H, 4.40; N, 6.43. Found (%): C, 64.54; H, 4.42; N, 6.40. M.p. 195 °C (dec.). Λ_M (acetone, 298 K): 166 Ohm^{-1} mol^{-1} cm^2. ^1H NMR ($CDCl_3$, 233 K) δ 8.55 (t, 1H, $^3J_{HH}$ = 7.7 Hz, py), 8.46 (d, 1H, $^3J_{HH}$ = 8.4 Hz, py), 8.34 (d, 1H, $^3J_{HH}$ = 8.6 Hz, btz), 8.08 (d, 1H, $^3J_{HH}$ = 8.5 Hz, btz), 8.04 (d, 1H, $^3J_{HH}$ = 4.8 Hz, py), 7.87 (t, 1H, $^3J_{HH}$ = 8.0 Hz, btz), 7.58 (t, 1H, $^3J_{HH}$ = 7.6 Hz, btz), 7.43 (t, 1H, $^3J_{HH}$ = 6.5 Hz, py), 7.34 (t, 6H, $^3J_{HH}$ = 7.0 Hz, phosphine), 7.25–7.05 (m, 24H, br, phosphine). $^{31}P\{^1H\}$ NMR ($CDCl_3$, 298 K) δ 2.40 (FWHM = 98 Hz). IR (KBr, cm^{-1}): 3130–3005 m/w (aromatic ν_{C-H}), 1610–1570 m/s (aromatic ν_{C-C} and ν_{C-N}), 1130–1000 s (ν_{BF_4}).

Characterization of $[Cu(pym\text{-}btz)(PPh_3)_2][BF_4]$ (2a). Anal. calcd for $C_{46}H_{37}BCuF_4N_5P_2$ (872.13 g mol^{-1}, %): C, 63.35; H, 4.28; N, 8.03. Found (%): C, 63.10; H, 4.30; N, 8.01. M.p. 155 °C. Λ_M (acetone, 298 K): 155 Ohm^{-1} mol^{-1} cm^2. ^1H NMR ($CDCl_3$, 298 K) δ 9.20–7.50 (broad signals, pym and btz), 7.40–7.15 (m, br, PPh_3). $^{31}P\{^1H\}$ NMR ($CDCl_3$, 298 K) δ 3.00 (FWHM = 94 Hz). IR (KBr, cm^{-1}): 3100–3060 m/w (aromatic ν_{C-H}), 1640–1570 m (aromatic ν_{C-C} and ν_{C-N}), 1120–1000 m (ν_{BF_4}).

Characterization of $[Cu(trz^{OMe}\text{-}btz)(PPh_3)_2][BF_4]$ (3a). Anal. calcd for $C_{47}H_{40}BCuF_4N_6O_2P_2$ (933.17 g mol^{-1}, %): C, 60.49; H, 4.32; N, 9.01. Found (%): C, 60.25; H, 4.34; N, 8.97. M.p. 115 °C. Λ_M (acetone, 298 K): 165 Ohm^{-1} mol^{-1} cm^2. ^1H NMR ($CDCl_3$, 243 K)

δ 8.48 (d, 1H, $^3J_{HH}$ = 8.4 Hz, btz), 8.15 (d, 1H, $^3J_{HH}$ = 8.4 Hz, btz), 7.89 (t, 1H, $^3J_{HH}$ = 7.7 Hz, btz), 7.66 (t, 1H, $^3J_{HH}$ = 7.7 Hz, btz), 7.40–7.16 (m, br, 30H, PPh_3), 4.35 (s, 3H, $-CH_3$), 3.91 (s, 3H, $-CH_3$). $^{31}P\{^1H\}$ NMR ($CDCl_3$, 298 K) δ 2.89 (FWHM = 97 Hz). IR (KBr, cm^{-1}): 3120–3005 (aromatic ν_{C-H}), 2990–2880 m/w (ν_{C-H}), 1620–1545 m (aromatic ν_{C-C} and ν_{C-N}), 1140–980 s (ν_{BF_4}).

Characterization of [Cu(trz^{OEt}-btz)(PPh_3)$_2$][BF_4] (4a). Anal. calcd for $C_{49}H_{44}BCuF_4N_6O_2P_2$ (961.23 g mol^{-1}, %): C, 61.23; H, 4.61; N, 8.74. Found (%): C, 60.59; H, 4.63; N, 8.71. M.p. 185 °C. Λ_M (acetone, 298 K): 160 Ohm^{-1} mol^{-1} cm^2. ^1H NMR ($CDCl_3$, 243 K) δ 8.46 (d, 1H, $^3J_{HH}$ = 8.4 Hz, btz), 8.14 (d, 1H, $^3J_{HH}$ = 8.4 Hz, btz), 7.90 (t, 1H, $^3J_{HH}$ = 7.7 Hz, btz), 7.66 (t, 1H, $^3J_{HH}$ = 7.7 Hz, btz), 7.40–7.15 (m, br, 30H, PPh_3), 4.77 (q, 2H, $^3J_{HH}$ = 7.2 Hz, $-CH_2$), 4.39 (q, 2H, $^3J_{HH}$ = 7.1 Hz, $-CH_2$), 1.60 (t, 3H, $^3J_{HH}$ = 7.2 Hz, $-CH_3$), 1.14 (t, 3H, $^3J_{HH}$ = 7.2 Hz, $-CH_3$). $^{31}P\{^1H\}$ NMR ($CDCl_3$, 298 K) δ 2.57 (FWHM = 84 Hz). IR (KBr, cm^{-1}): 3105–3000 m/w (aromatic ν_{C-H}), 2980–2850 m/w (ν_{C-H}), 1640–1580 m (aromatic ν_{C-C} and ν_{C-N}), 1110–995 s (ν_{BF_4}).

Characterization of [Cu(trz^{OPh}-btz)(PPh_3)$_2$][BF_4] (5a). Anal. calcd for $C_{57}H_{44}BCuF_4N_6O_2P_2$ (1057.32 g mol^{-1}, %): C, 64.75; H, 4.19; N, 7.95. Found (%): C, 64.49; H, 4.21; N, 7.92. M.p. 90 °C. Λ_M (acetone, 298 K): 149 Ohm^{-1} mol^{-1} cm^2. ^1H NMR ($CDCl_3$, 243 K) δ 8.14 (d, 1H, $^3J_{HH}$ = 8.3 Hz, btz), 8.10 (d, 1H, $^3J_{HH}$ = 8.1 Hz, btz), 7.80–6.50 (m, 42H, btz, Ph and PPh_3). $^{31}P\{^1H\}$ NMR ($CDCl_3$, 298 K) δ 3.01 (FWHM = 184 Hz). IR (KBr, cm^{-1}): 3105–3010 m/w (aromatic ν_{C-H}), 1620–1550 m (aromatic ν_{C-C} and ν_{C-N}); 1115–1000 m (ν_{BF_4}).

Synthesis and characterization of complexes 1b–4b, 1c–5c and 1d–5d

To a solution containing 0.472 g of $[Cu(NCCH_3)_4][BF_4]$ (1.5 mmol) in 20 mL of dry CH_2Cl_2, 3.0 mmol of P^iPr_3 (4.81 g of 10% solution in hexane) or 1.5 mmol of dppe (0.598 g) or DPEphos (0.808 g) were added. After 4 hours, 1.5 mmol of the proper ligand was added. After stirring overnight, the solvent was evaporated under reduced pressure. The product was precipitated by the addition of Et_2O and the solid was filtered, washed and dried *in vacuo*. Yield > 75% in all the cases.

Characterization of [Cu(py-btz)(P^iPr_3)$_2$][BF_4] (1b). Anal. calcd for $C_{29}H_{50}BCuF_4N_4P_2$ (667.04 g mol^{-1}, %): C, 52.22; H, 7.56; N, 8.40. Found (%): C, 52.01; H, 7.59; N, 8.37. M.p. 135 °C (dec.). Λ_M (acetone, 298 K): 148 Ohm^{-1} mol^{-1} cm^2. ^1H NMR ($CDCl_3$, 298 K) δ 8.71 (d, 1H, $^3J_{HH}$ = 4.6 Hz, py), 8.60 (d, 1H, $^3J_{HH}$ = 8.3 Hz, btz), 8.36 (d, 1H, $^3J_{HH}$ = 8.5 Hz, py), 8.23 (t, 1H, $^3J_{HH}$ = 8.0 Hz, py), 8.19 (d, 1H, $^3J_{HH}$ = 8.3 Hz, btz), 7.76 (t, 1H, $^3J_{HH}$ = 7.7 Hz, btz), 7.59–7.51 (m, 2H, btz and py), 2.27 (m, br, 3H, CH-P^iPr_3), 1.29 (m, 18H, CH_3-P^iPr_3). $^{31}P\{^1H\}$ NMR ($CDCl_3$, 298 K) δ 27.87 (FWHM = 75 Hz). IR (KBr, cm^{-1}): IR (KBr, cm^{-1}): 3110–2870 m/w (aromatic ν_{C-H} and ν_{C-H}), 1640–1560 m (aromatic ν_{C-C} and ν_{C-N}), 1160–1020 m (ν_{BF_4}).

Characterization of [Cu(pym-btz)(P^iPr_3)$_2$][BF_4] (2b). Anal. calcd for $C_{28}H_{49}BCuF_4N_5P_2$ (668.03 g mol^{-1}, %): C, 50.34; H, 7.39; N, 10.48. Found (%): C, 50.14; H, 7.42; N, 10.44. M.p. 115 °C (dec.). Λ_M (acetone, 298 K): 88 Ohm^{-1} mol^{-1} cm^2. ^1H NMR ($CDCl_3$, 298 K) δ 9.17 (d, 2H, $^3J_{HH}$ = 5.0 Hz, pym), 8.74 (d, 1H, $^3J_{HH}$ = 8.4 Hz, btz), 8.24 (d, 1H, $^3J_{HH}$ = 8.4 Hz, btz), 7.98 (t, 1H, $^3J_{HH}$ = 5.0 Hz, pym), 7.83 (td, 1H, $^3J_{HH}$ = 7.9 Hz, btz), 7.65 (td, 1H, $^3J_{HH}$ = 8.0 Hz, btz), 2.15 (m, br, 3H, CH-P^iPr_3), 1.20 (m, br, 18H, CH_3-P^iPr_3). $^{31}P\{^1H\}$ NMR ($CDCl_3$, 298 K) δ 21.80 (FWHM = 120 Hz). IR (KBr, cm^{-1}): 3100–2870 m/w (aromatic ν_{C-H} and ν_{C-H}), 1640–1570 m (aromatic ν_{C-C} and ν_{C-N}), 1150–1000 m (ν_{BF_4}).

Characterization of [Cu(trz^{OMe}-btz)(P^iPr_3)$_2$][BF_4] (3b). Anal. calcd for $C_{29}H_{52}BCuF_4N_6O_2P_2$ (729.07 g mol^{-1}, %): C, 47.78; H, 7.19; N, 11.53. Found (%): C, 47.59; H, 7.22; N, 11.48. M.p. 155 °C (dec.). Λ_M (acetone, 298 K): 195 Ohm^{-1} mol^{-1} cm^2. ^1H NMR ($CDCl_3$, 243 K) δ 8.59 (d, 1H, $^3J_{HH}$ = 8.4 Hz, btz), 8.23 (d, 1H, $^3J_{HH}$ = 8.4 Hz, btz), 7.78 (t, 1H, $^3J_{HH}$ = 7.8 Hz, btz), 7.61 (t, 1H, $^3J_{HH}$ = 7.8 Hz, btz), 4.29 (s, 6H, $-CH_3$), 2.18 (m, 3H, CH-P^iPr_3), 1.28 (m, 18H, CH_3-P^iPr_3). $^{31}P\{^1H\}$ NMR ($CDCl_3$, 298 K) δ 40.12 (FWHM = 3 Hz). IR (KBr, cm^{-1}): 3078 w (aromatic ν_{C-H}), 2960–2870 m/w (ν_{C-H}), 1615–1540 m (aromatic ν_{C-C} and ν_{C-N}), 1140–1020 (ν_{BF_4}).

Characterization of [Cu(trz^{OEt}-btz)(P^iPr_3)$_2$][BF_4] (4b). Anal. calcd for $C_{31}H_{56}BCuF_4N_6O_2P_2$ (757.13 g mol^{-1}, %): C, 49.18; H, 7.46; N, 11.10. Found (%): C, 48.98; H, 7.49; N, 11.07. M.p. 145 °C (dec.). Λ_M (acetone, 298 K): 207 Ohm^{-1} mol^{-1} cm^2. ^1H NMR ($CDCl_3$, 298 K) δ 8.59 (d, 1H, $^3J_{HH}$ = 8.4 Hz, btz), 8.16 (d, 1H, $^3J_{HH}$ = 8.4 Hz, btz), 7.83 (t, 1H, $^3J_{HH}$ = 7.8 Hz, btz), 7.63 (t, 1H, $^3J_{HH}$ = 7.7 Hz, btz), 4.76 (q, 4H, $^3J_{HH}$ = 7.4 Hz, $-CH_2$), 2.29 (m, 3H, CH-P^iPr_3), 1.56 (t, 6H, $^3J_{HH}$ = 7.4 Hz, $-CH_3$), 1.38 (m, br, 18H, CH_3- P^iPr_3). $^{31}P\{^1H\}$ NMR ($CDCl_3$, 298 K) δ 37.65 (FWHM = 83 Hz). IR (KBr, cm^{-1}): 3120–3070 m/w (aromatic ν_{C-H}), 2980–2870 m/w (ν_{C-H}), 1620–1540 m/s (aromatic ν_{C-C} and ν_{C-N}), 1180–1020 s (ν_{BF_4}).

Characterization of [Cu(py-btz)(μ-dppe)]$_2$[BF_4]$_2$ (1c)

Anal. calcd for $C_{74}H_{64}B_2Cu_2F_8N_8P_4$ (1489.98 g mol^{-1}, %): C, 59.65; H, 4.33; N, 7.52. Found (%): C, 59.42; H, 4.35; N, 7.49. M.p. 115 °C (dec.). Λ_M (acetone, 298 K): 316 Ohm^{-1} mol^{-1} cm^2. ^1H NMR ($CDCl_3$, 298 K) δ 8.76 (d, 1H, $^3J_{HH}$ = 8.4 Hz, py), 8.70–8.55 (m, 2H, py and btz), 8.37 (d, 1H, $^3J_{HH}$ = 8.2 Hz, btz), 8.05 (d, 1H, $^3J_{HH}$ = 5.0 Hz, py), 8.00 (t, 1H, $^3J_{HH}$ = 8.1 Hz, btz), 7.73 (t, 1H, $^3J_{HH}$ = 7.7 Hz, btz), 7.67–7.13 (m, 21H, btz and Ph), 2.66 (m, 2H, dppe), 2.50 (m, 2H, dppe). $^{31}P\{^1H\}$ NMR ($CDCl_3$, 213 K) δ −4.55 (FWHM = 30 Hz). IR (KBr, cm^{-1}): 3070–2850 m/w (aromatic ν_{C-H} and ν_{C-H}), 1640–1560 m (aromatic ν_{C-C} and ν_{C-N}), 1140–1020 m (ν_{BF_4}).

Characterization of [Cu(pym-btz)(μ-dppe)]$_2$[BF_4]$_2$ (2c). Anal. calcd for $C_{72}H_{62}B_2Cu_2F_8N_{10}P_4$ (1491.96 g mol^{-1}, %): C, 57.96; H, 4.19; N, 9.39. Found (%): C, 57.73; H, 4.21; N, 9.35. M.p. 189 °C (dec.). Λ_M (acetone, 298 K): 308 Ohm^{-1} mol^{-1} cm^2. ^1H NMR ($CDCl_3$, 273 K) δ 9.18 (s, 1H, pym), 9.06 (s, 1H, pym), 8.80 (d, 1H, $^3J_{HH}$ = 8.2 Hz, btz), 8.33 (d, 1H, $^3J_{HH}$ = 8.3 Hz, btz), 7.95 (t, 1H, $^3J_{HH}$ = 4.7 Hz, pym), 7.89 (t, 1H, $^3J_{HH}$ = 7.9 Hz, btz), 7.72 (t, 1H, $^3J_{HH}$ = 7.9 Hz, btz), 7.68–7.10 (m, 20H, dppe), 2.71 (m, 2H, dppe), 2.45 (m, 2H, dppe). $^{31}P\{^1H\}$ NMR ($CDCl_3$, 298 K) δ −3.61 (FWHM = 129 Hz). IR (KBr, cm^{-1}): 3100–3025 m/w (aromatic ν_{C-H}), 2970–2850 *w* (ν_{C-H}), 1640–1570 m (aromatic ν_{C-C} and ν_{C-N}), 1120–1000 m (ν_{BF_4}).

Characterization of [Cu(trz^{OMe}-btz)(μ-dppe)]$_2$[BF_4]$_2$ (3c). Anal. calcd for $C_{74}H_{68}B_2Cu_2F_8N_{12}O_4P_4$ (1614.04 g mol^{-1}, %):

C, 55.07; H, 4.25; N, 10.41. Found (%): C, 54.85; H, 4.27; N, 10.37. M.p. 217 °C (dec.). Λ_M (acetone, 298 K): 332 Ohm^{-1} mol^{-1} cm^2. ^1H NMR ($CDCl_3$, 298 K) δ 9.00–7.00 (m, br, 24H, btz and dppe), 4.37 (s, 3H, $-CH_3$), 4.25 (s, 3H, $-CH_3$), 2.90–2.30 (m, 4H, dppe). $^{31}P\{^1H\}$ NMR ($CDCl_3$, 298 K) δ −3.36 (FWHM = 117 Hz). IR (KBr, cm^{-1}): 3110–3005 m/w (aromatic ν_{C-H}), 2960–2850 m/w (ν_{C-H}), 1620–1530 m/s (aromatic ν_{C-C} and ν_{C-N}), 1120–995 s (ν_{BF_4}).

Characterization of [Cu(trz^{OEt}-btz)(μ-dppe)]$_2$[BF$_4$]$_2$ (4c). Anal. calcd for $C_{78}H_{76}B_2Cu_2F_8N_{12}O_4P_4$ (1670.14 g mol^{-1}, %): C, 56.09; H, 4.59; N, 10.06. Found (%): C, 55.87; H, 4.61; N, 10.02. M.p. 220 °C (dec.). Λ_M (acetone, 298 K): 328 Ohm^{-1} mol^{-1} cm^2. ^1H NMR ($CDCl_3$, 233 K) δ 8.70 (d, 1H, $^3J_{HH}$ = 8.4 Hz, btz), 8.41 (d, 1H, $^3J_{HH}$ = 8.4 Hz, btz), 8.00 (t, 1H, $^3J_{HH}$ = 7.8 Hz, btz), 7.79 (t, 1H, $^3J_{HH}$ = 7.8 Hz, btz), 7.65–7.05 (m, br, 40H, dppe), 4.83 (q, 2H, $^3J_{HH}$ = 7.0 Hz, $-CH_2$), 4.01 (q, 2H, $^3J_{HH}$ = 7.0 Hz, $-CH_2$), 2.66 (m, br, 4H, dppe), 2.43 (m, br, 4H, dppe), 1.62 (t, 3H, $^3J_{HH}$ = 7.1 Hz, $-CH_3$), 0.58 (t, 6H, J_{HH} = 7.1 Hz, $-CH_3$). $^{31}P\{^1H\}$ NMR ($CDCl_3$, 298 K) δ −3.60 (FWHM = 111 Hz). IR (KBr, cm^{-1}): 3075–2850 m/w (aromatic ν_{C-H} and ν_{C-H}), 1620–1530 m/s (aromatic ν_{C-C} and ν_{C-N}), 1180–950 s (ν_{BF_4}).

Characterization of [Cu(trz^{OPh}-btz)(μ-dppe)]$_2$[BF$_4$]$_2$ (5c). Anal. calcd for $C_{94}H_{76}B_2Cu_2F_8N_{12}O_4P_4$ (1862.32 g mol^{-1}, %): C, 60.63; H, 4.11; N, 9.03. Found (%): C, 60.39; H, 4.13; N, 8.99. M.p. 140 °C (dec.). Λ_M (acetone, 298 K): 314 Ohm^{-1} mol^{-1} cm^2. ^1H NMR ($CDCl_3$, 213 K) δ 8.26 (d, 1H, $^3J_{HH}$ = 8.3 Hz, btz), 7.90–7.05 (m, br, 31H, btz, dppe and Ph), 6.39 (d, 2H, $^3J_{HH}$ = 7.6 Hz, Ph), 2.67 (m, br, 2H, dppe), 2.37 (m, br, 2H, dppe). $^{31}P\{^1H\}$ NMR ($CDCl_3$, 298 K) δ −3.74 (FWHM = 86 Hz). IR (KBr, cm^{-1}): 3100–3020 m/w (aromatic ν_{C-H}), 2920–2850 m/w (ν_{C-H}), 1620–1550 m/s (aromatic ν_{C-C} and ν_{C-N}), 1110–1000 m (ν_{BF_4}).

Characterization of [Cu(py-btz)(DPEphos)][BF$_4$] (1d). Anal. calcd for $C_{47}H_{36}BCuF_4N_4OP_2$ (885.13 g mol^{-1}, %): C, 63.78; H, 4.10; N, 6.33. Found (%): C, 63.52; H, 4.12; N, 6.31. M.p. 215 °C (dec.). Λ_M (acetone, 298 K): 166 Ohm^{-1} mol^{-1} cm^2. ^1H NMR ($CDCl_3$, 233 K) δ 8.53 (t, 1H, $^3J_{HH}$ = 8.0 Hz, py), 8.47 (d, 1H, $^3J_{HH}$ = 8.3 Hz, py), 8.32 (d, 1H, $^3J_{HH}$ = 8.6 Hz, btz), 8.02 (d, 1H, $^3J_{HH}$ = 8.7 Hz, btz), 7.93 (d, 1H, $^3J_{HH}$ = 4.5 Hz, py), 7.82 (t, 1H, $^3J_{HH}$ = 7.7 Hz, btz), 7.60–7.55 (m, 30H, br, btz and py and DPEphos). $^{31}P\{^1H\}$ NMR ($CDCl_3$, 273 K) δ −11.30 (FWHM = 78 Hz). IR (KBr, cm^{-1}): 3070–3015 m/w (aromatic ν_{C-H}), 1610–1560 m/s (aromatic ν_{C-C} and ν_{C-N}), 1130–1020 s (ν_{BF_4}).

Characterization of [Cu(pym-btz)(DPEphos)][BF$_4$] (2d). Anal. calcd for $C_{46}H_{35}BCuF_4N_5OP_2$ (886.12 g mol^{-1}, %): C, 62.35; H, 3.98; N, 7.90. Found (%): C, 62.10; H, 4.00; N, 7.87. M.p. > 230 °C. Λ_M (acetone, 298 K): 158 Ohm^{-1} mol^{-1} cm^2. ^1H NMR ($CDCl_3$, 298 K) δ 9.18 (s, br, 1H, pym), 8.60 (d, 1H, $^3J_{HH}$ = 8.2 Hz, btz), 8.38 (s, br, 1H, pym), 8.11 (d, 1H, $^3J_{HH}$ = 8.5 Hz, btz), 7.79 (t, 1H, $^3J_{HH}$ = 7.7 Hz, btz), 7.74 (t, 1H, $^3J_{HH}$ = 5.0 Hz, pym), 7.60 (t, 1H, $^3J_{HH}$ = 7.8 Hz, btz), 7.50–6.80 (m, 28H, br, DPEphos). $^{31}P\{^1H\}$ NMR ($CDCl_3$, 298 K) δ −11.10 (FWHM = 98 Hz). IR (KBr, cm^{-1}): 3100–3010 m/w (aromatic ν_{C-H}), 1640–1570 m (aromatic ν_{C-C} and ν_{C-N}), 1130–1020 m (ν_{BF_4}).

Characterization of [Cu(trz^{OMe}-btz)(DPEphos)][BF$_4$] (3d). Anal. calcd for $C_{47}H_{38}BCuF_4N_6O_3P_2$ (947.16 g mol^{-1}, %): C, 59.60; H, 4.04; N, 8.87. Found (%): C, 59.36; H, 4.06; N, 8.83. M.p. 225 °C (dec.). Λ_M (acetone, 298 K): 118 Ohm^{-1} mol^{-1} cm^2. ^1H NMR ($CDCl_3$, 243 K) δ 8.53 (d, 1H, $^3J_{HH}$ = 8.3 Hz, btz), 8.16 (d, 1H, $^3J_{HH}$ = 8.3 Hz, btz), 7.89 (t, 1H, $^3J_{HH}$ = 7.7 Hz, btz), 7.65 (t, 1H, $^3J_{HH}$ = 7.7 Hz, btz), 7.45–7.15 (m, br, 22H, DPEphos), 7.05–6.90 (m, br, 4H, DPEphos), 6.80–6.70 (m, br, 2H, DPEphos), 4.37 (s, 6H, $-CH_3$). $^{31}P\{^1H\}$ NMR ($CDCl_3$, 298 K) δ −11.43 (FWHM = 103 Hz). IR (KBr, cm^{-1}): 3120–3005 m/w (aromatic ν_{C-H}), 2980–2860 m/w (ν_{C-H}), 1620–1540 m/s (aromatic ν_{C-C} and ν_{C-N}), 1130–1000 s (ν_{BF_4}).

Characterization of [Cu(trz^{OEt}-btz)(DPEphos)][BF$_4$] (4d). Anal. calcd for $C_{49}H_{42}BCuF_4N_6O_3P_2$ (975.21 g mol^{-1}, %): C, 60.35; H, 4.34; N, 8.62. Found (%): C, 60.11; H, 4.36; N, 8.59. M.p. > 230 °C. Λ_M (acetone, 298 K): 170 Ohm^{-1} mol^{-1} cm^2. ^1H NMR ($CDCl_3$, 243 K) δ 8.47 (d, 1H, $^3J_{HH}$ = 8.3 Hz, btz), 8.19 (d, 1H, $^3J_{HH}$ = 8.3 Hz, btz), 7.89 (t, 1H, $^3J_{HH}$ = 7.7 Hz, btz), 7.66 (t, 1H, $^3J_{HH}$ = 7.7 Hz, btz), 7.50–6.70 (m, br, 28H, DPEphos), 4.79 (q, 2H, $^3J_{HH}$ = 7.0 Hz, $-CH_2$), 4.03 (q, 2H, $^3J_{HH}$ = 7.0 Hz, $-CH_2$), 1.62 (t, 3H, $^3J_{HH}$ = 7.0 Hz, $-CH_3$), 0.64 (t, 6H, $^3J_{HH}$ = 7.0 Hz, $-CH_3$). $^{31}P\{^1H\}$ NMR ($CDCl_3$, 298 K) δ −11.83 (FWHM = 83 Hz). IR (KBr, cm^{-1}): 3070–3050 m/w (aromatic ν_{C-H}), 2980–2850 m/w (ν_{C-H}), 1620–1540 m/s (aromatic ν_{C-C} and ν_{C-N}), 1110–995 s (ν_{BF_4}).

Characterization of [Cu(trz^{OPh}-btz)(DPEphos)][BF$_4$] (5d). Anal. calcd for $C_{57}H_{42}BCuF_4N_6O_3P_2$ (1071.28 g mol^{-1}, %): C, 63.91; H, 3.95; N, 7.84. Found (%): C, 63.65; H, 3.97; N, 7.81. M.p. 150 °C (dec.). Λ_M (acetone, 298 K): 155 Ohm^{-1} mol^{-1} cm^2. ^1H NMR ($CDCl_3$, 313 K) δ 8.11 (m, 1H, btz), 7.80–6.50 (m, 41H, btz, Ph and DPEphos). $^{31}P\{^1H\}$ NMR ($CDCl_3$, 298 K) δ −11.70 (FWHM = 95 Hz). IR (KBr, cm^{-1}): 3070–3050 m/w (aromatic ν_{C-H}), 1620–1560 m/s (aromatic ν_{C-C} and ν_{C-N}), 1115–1000 m (ν_{BF_4}).

Author contributions

Jesús Castro: formal analysis, investigation, supervision, validation, writing – original draft, writing – review & editing. Valentina Ferraro: formal analysis, investigation, validation, writing – original draft, writing – review & editing. Marco Bortoluzzi: conceptualization, formal analysis, funding acquisition, supervision, writing – original draft, writing – review & editing.

Conflicts of interest

There are no conflicts to declare.

Acknowledgements

Università Ca' Foscari Venezia is gratefully acknowledged for financial support (Bando Spin 2018, D. R. 1065/2018 prot. 67416). CACTI (University of Vigo) and Cineca (Bologna) are gratefully acknowledged for X-ray data collection and availability of high-performance computer resources (class C project COLUMN21). We sincerely thank Dr Andrea Morandini for the advice on triazine chemistry.

Notes and references

1 O. S. Wenger, *J. Am. Chem. Soc.*, 2018, **140**, 13522–13533, DOI: 10.1021/jacs.8b08822.
2 Q.-C. Zhang, H. Xiao, X. Zhang, L.-J. Xu and Z.-N. Chen, *Coord. Chem. Rev.*, 2019, **378**, 121–133, DOI: 10.1016/j.ccr.2018.01.017.
3 R. D. Costa, E. Ortí, H. J. Bolink, F. Monti, G. Accorsi and N. Armaroli, *Angew. Chem., Int. Ed.*, 2012, **51**, 8178–8211, DOI: 10.1002/anie.201201471.
4 C. Bizzarri, E. Spuling, D. M. Knoll, D. Volz and S. Bräse, *Coord. Chem. Rev.*, 2018, **373**, 49–82, DOI: 10.1016/j.ccr.2017.09.011.
5 M. Freitag, J. Teuscher, Y. Saygili, X. Zhang, F. Giordano, P. Liska, J. Hua, S. M. Zakeeruddin, J.-E. Moser, M. Grätzel and A. Hagfeldt, *Nature Photon*, 2017, **11**, 372–378, DOI: 10.1038/nphoton.2017.60.
6 C. Wegeberg and O. S. Wenger, *JACS Au*, 2021, **1**, 1860–1876, DOI: 10.1021/jacsau.1c00353.
7 X. Li, Y. Xie and Z. Li, *Chem. – Asian J.*, 2021, **16**, 2817–2829, DOI: 10.1002/asia.202100784.
8 L. M. Cavinato, S. Wölfl, A. Pöthig, E. Fresta, C. Garino, J. Fer-nandez-Cestau, C. Barolo and R. D. Costa, *Adv. Mater.*, 2022, **34**, 2109228, DOI: 10.1002/adma.202109228.
9 Y. Zhang, M. Schulz, M. Wächtler, M. Karnahl and B. Dietzek, *Coord. Chem. Rev.*, 2018, **356**, 127–146, DOI: 10.1016/j.ccr.2017.10.016.
10 P. A. Forero Cortés, M. Marx, M. Trose and M. Beller, *Chem. Catalysis*, 2021, **1**, 298–338, DOI: 10.1016/j.checat.2021.05.005.
11 C. Bizzarri, *Eur. J. Org. Chem.*, 2022, e202200185, DOI: 10.1002/ejoc.202200185.
12 C. Förster and K. Heize, *Chem. Soc. Rev.*, 2020, **49**, 1057–1070, DOI: 10.1039/c9cs00573k.
13 E. Mejía, S.-P. Luo, M. Karnahl, A. Friedrich, S. Tschierlei, A.-E. Surkus, H. Junge, S. Gladiali, S. Lochbrunner and M. Beller, *Chem. – Eur. J.*, 2013, **19**, 15972–15978, DOI: 10.1002/chem.201302091.
14 P.-T. Chou and Y. Chi, *Chem. – Eur. J.*, 2007, **13**, 380–395, DOI: 10.1002/chem.200601272.
15 W.-P. To, Q. Wan, G. S. Ming Tong and C.-M. Che, *Trends Chem.*, 2020, **2**, 796–812, DOI: 10.1016/j.trechm.2020.06.004.
16 H. Xu, R. Chen, Q. Sun, W. Lai, Q. Su, W. Huang and X. Liu, *Chem. Soc. Rev.*, 2014, **43**, 3259–3302, DOI: 10.1039/C3CS60449G.
17 K.-H. Kim and J.-J. Kim, *Adv. Mater.*, 2018, **30**, 1705600, DOI: 10.1002/adma.201705600.
18 W. C. H. Choy, W.-K. Chan and Y. Yuan, *Adv. Mater.*, 2014, **26**, 5368–5399, DOI: 10.1002/adma.201306133.
19 K. Li, Y. Chen, J. Wang and C. Yang, *Coord. Chem. Rev.*, 2021, **433**, 213755, DOI: 10.1016/j.ccr.2020.213755.
20 Y. Tao, K. Yuan, T. Chen, P. Xu, H. Li, R. Chen, C. Zheng, L. Zhang and W. Huang, *Adv. Mater.*, 2014, **26**, 7931–7958, DOI: 10.1002/adma.201402532.
21 H. Yersin, A. F. Rausch, R. Czerwieniec, T. Hofbeck and T. Fischer, *Coord. Chem. Rev.*, 2011, **255**, 2622–2652, DOI: 10.1016/j.ccr.2011.01.042.
22 H. Yersin, *Highly Efficient OLEDs: Materials Based on Thermally Activated Delayed Fluorescence*, Wiley-VCH, Weinheim, 2018.
23 G. U. Mahoro, J. Fernandez-Cestau, J.-C. Renaud, P. B. Coto, R. D. Costa and S. Gaillard, *Adv. Optical Mater*, 2020, **8**, 2000260, DOI: 10.1002/adom.202000260.
24 C. Sandoval-Pauker, M. Santander-Nelli and P. Dreyse, *RSC Adv.*, 2022, **12**, 10653–10674, DOI: 10.1039/D1RA08082B.
25 Y. Liu, S.-C. You, C.-L. Ho and W.-Y. Wong, *Chem. Coord. Rev.*, 2018, **375**, 514–557, DOI: 10.1016/j.ccr.2018.05.010.
26 M. S. Lazorski and F. N. Castellano, *Polyhedron*, 2014, **82**, 57–70, DOI: 10.1016/j.poly.2014.04.060.
27 D. V. Scaltrito, D. W. Thompson, J. A. O'Callaghan and G. J. Meyer, *Coord. Chem. Rev.*, 2000, **208**, 243–266, DOI: 10.1016/S0010-8545(00)00309-X.
28 A. Lavie-Cambot, M. Cantuel, Y. Leydet, G. Jonusauskas, D. M. Bassani and N. D. McClenaghan, *Coord. Chem. Rev.*, 2008, **252**, 2572–2584, DOI: 10.1016/j.ccr.2008.03.013.
29 T. Tsubomura, K. Kimura, M. Nishikawa and T. Tsukuda, *Dalton Trans.*, 2015, **44**, 7554–7562, DOI: 10.1039/C5DT00835B.
30 E. Leoni, J. Mohanraj, M. Holler, M. Mohankumar, I. Nierengarten, F. Monti, A. Sournia-Saquet, B. Delavaux-Nicot, J.-F. Nierengarten and N. Armaroli, *Inorg. Chem.*, 2018, **57**, 15537–15549, DOI: 10.1021/acs.inorgchem.8b02879.
31 S. Saeedi, C. Xue, B. J. McCullough, S. E. Roe, B. J. Neyhouse and T. White, *ACS Appl. Energy Mater.*, 2019, **2**, 131–143, DOI: 10.1021/acsaem.8b02098.
32 S. Keller, A. Pertegás, G. Longo, L. Martínez, J. Cerdá, J. M. Junquera-Hernández, A. Prescimone, E. C. Constable, C. E. Housecroft, E. Ortí and H. J. Bolink, *J. Mater. Chem. C*, 2016, **4**, 3857–3871, DOI: 10.1039/C5TC03725E.
33 L.-X. Xu, T.-Q. Wang, X.-F. Liu, H. Chen, C.-J. Wei, D. D. Xu, F. Chen, Y. Li and S.-P. Luo, *Eur. J. Inorg. Chem.*, 2020, 4278–4283, DOI: 10.1002/ejic.202000648.
34 F. Doettinger, Y. Yang, M.-A. Schmid, W. Frey, M. Karnahl and S. Tschierlei, *Inorg. Chem.*, 2021, **60**, 5391–5401, DOI: 10.1021/acs.inorgchem.1c00416.
35 Z. Si, J. Li, B. Li, S. Liu and W. Li, *J. Lumin.*, 2009, **129**, 181–186, DOI: 10.1016/j.jlumin.2008.09.014.
36 J. Min, Q. Zhang, W. Sun, Y. Cheng and L. Wang, *Dalton Trans.*, 2011, **40**, 686–693, DOI: 10.1039/C0DT01031F.
37 O. Back, J. Leppin, C. Förster and K. Heinze, *Inorg. Chem.*, 2016, **55**, 9653–9662, DOI: 10.1021/acs.inorgchem.6b01400.
38 C. Femoni, S. Muzzioli, A. Palazzi, S. Stagni, S. Zacchini, F. Monti, G. Accorsi, M. Bolognesi, N. Armaroli, M. Massi, G. Valenti and M. Marcaccio, *Dalton Trans.*, 2013, **42**, 997–1010, DOI: 10.1039/C2DT32056H.
39 L. Bergmann, C. Braun, M. Nieger and S. Bräse, *Dalton Trans.*, 2018, **47**, 608–621, DOI: 10.1039/C7DT03682E.
40 J.-L. Chen, P. Song, J. Liao, H.-R. Wen, R. Hong, Z.-N. Chen and Y. Chic, *Inorg. Chem. Commun.*, 2010, **13**, 1057–1060, DOI: 10.1016/j.inoche.2010.06.010.
41 J.-L. Chen, Z.-H. Guo, H.-G. Yu, L.-H. He, S.-J. Liu, H.-R. Wen and J.-Y. Wang, *Dalton Trans.*, 2016, **45**, 696–705, DOI: 10.1039/C5DT03451E.

42 A. Alconchel, O. Crespo, P. García-Orduña and M. Concepción Gimeno, *Inorg. Chem.*, 2021, **60**, 18521–18528, DOI: **10.1021/acs.inorgchem.1c03092**.
43 K. F. Baranova, A. A. Titov, A. F. Smol'yakov, A. Y. Chernyadyev, O. A. Filippov and E. S. Shubina, *Molecules*, 2021, **26**, 6869, DOI: **10.3390/molecules26226869**.
44 M. Grupe, P. Boden, P. Di Martino-Fumo, X. Gui, C. Bruschi, R. Israil, M. Schmitt, M. Nieger, M. Gerhards, W. Klopper, C. Riehn, C. Bizzarri and R. Diller, *Chem. – Eur. J.*, 2021, **27**, 15252–15271, DOI: **10.1002/chem.202102760**.
45 Y. Wu, X. Han, Y. Qu, K. Zhao, C. Wang, G. Huang and H. Wu, *J. Mol. Struct.*, 2019, **1191**, 95–100, DOI: **10.1016/j.molstruc.2019.04.108**.
46 B. Hupp, C. Schiller, C. Lenczyk, M. Stanoppi, K. Edkins, A. Lorbach and A. Steffen, *Inorg. Chem.*, 2017, **56**, 8996–9008, DOI: **10.1021/acs.inorgchem.7b00958**.
47 L. Pathaw, D. Maheshwaran, T. Nagendraraj, T. Khamrang, M. Velusamy and R. Mayilmurugan, *Inorg. Chim. Acta*, 2021, **514**, 119999, DOI: **10.1016/j.ica.2020.119999**.
48 C. Bizzarri, A. P. Arndt, S. Kohaut, K. Fink and M. Nieger, *J. Organomet. Chem.*, 2018, **871**, 140–149, DOI: **10.1016/j.jorganchem.2018.07.013**.
49 G. Li, R. S. Nobuyasu, B. Zhang, Y. Geng, B. Yao, Z. Xie, D. Zhu, G. Shan, W. Che, L. Yan, Z. Su, F. B. Dias and M. R. Bryce, *Chem. – Eur. J.*, 2017, **23**, 11761–11766, DOI: **10.1002/chem.201701862**.
50 Y. Sun, V. Lemaur, J. I. Beltrán, J. Cornil, J. Huang, J. Zhu, Y. Wang, R. Fröhlich, H. Wang, L. Jiang and G. Zou, *Inorg. Chem.*, 2016, **55**, 5845–5852, DOI: **10.1021/acs.inorgchem.6b00101**.
51 Q. Zhang, X.-L. Chen, J. Chen, X.-Y. Wu, R. Yu and C.-Z. Lu, *Dalton Trans.*, 2015, **44**, 10022–10029, DOI: **10.1039/C5DT01108F**.
52 L. Bergmann, J. Friedrichs, M. Mydlak, T. Baumann, M. Nieger and S. Bräse, *Chem. Commun.*, 2013, **49**, 6501–6503, DOI: **10.1039/C3CC42280A**.
53 C.-W. Hsu, C.-C. Lin, M.-W. Chung, Y. Chi, G.-H. Lee, P.-T. Chou, C.-H. Chang and P.-Y. Chen, *J. Am. Chem. Soc.*, 2011, **133**, 12085–12099, DOI: **10.1021/ja2026568**.
54 N. Lüdtke, J. Föller and C. M. Marian, *Phys. Chem. Chem. Phys.*, 2020, **22**, 23530–23544, DOI: **10.1039/d0cp04654j**.
55 E. Loukopoulos and G. E. Kostakis, *Coord. Chem. Rev.*, 2019, **395**, 193–229, DOI: **10.1016/j.ccr.2019.06.003**.
56 R. Gérardy and J.-C. M. Monbaliu, *Top. Heterocycl. Chem.*, 2015, **43**, 1–66, DOI: **10.1007/7081_2015_179**.
57 A. R. Katritzky and B. V. Rogovoy, *Chem. – Eur. J.*, 2003, **9**, 4586–4593, DOI: **10.1002/chem.200304990**.
58 M. Bortoluzzi, J. Castro, M. Girotto, F. Enrichi and A. Vomiero, *Inorg. Chem. Commun.*, 2019, **102**, 141–146, DOI: **10.1016/j.inoche.2019.02.016**.
59 V. Ferraro, M. Bortoluzzi, J. Castro, A. Vomiero and S. You, *Inorg. Chem. Commun.*, 2020, **116**, 107894, DOI: **10.1016/j.inoche.2020.107894**.
60 V. Ferraro, J. Castro, L. Agostinis and M. Bortoluzzi, *Transit. Met. Chem*, 2021, **46**, 391–402, DOI: **10.1007/s11243-021-00458-4**.
61 A. R. Katritzky and J. Wu, *Synthesis*, 1994, 597–600, DOI: **10.1055/s-1994-25530**.
62 A. R. Katritzky, A. V. Ignatchenko and H. Lang, *Heterocycles*, 1995, **4**, 131–146, DOI: **10.3987/COM-94-6918**.
63 V. Ferraro, J. Castro, E. Trave and M. Bortoluzzi, *J. Organomet. Chem.*, 2022, **957**, 122171, DOI: **10.1016/j.jorganchem.2021.122171**.
64 K. Nakamoto, *Infrared and Raman Spectra of Inorganic and Coordination Compounds. Part B: Applications in Coordination, Organometallic, and Bioinorganic Chemistry*, Wiley-VHC, Hoboken, 2009.
65 C. Li, C. F. R. Mackenzie, S. A. Said, A. K. Pal, M. A. Haghighatbin, A. Babaei, M. Sessolo, D. B. Cordes, A. M. Z. Slawin, P. C. J. Kamer, H. J. Bolink, C. F. Hogan and E. Zysman-Colman, *Inorg. Chem.*, 2021, **60**, 10323–10339, DOI: **10.1021/acs.inorgchem.1c00804**.
66 F. Mazzeo, F. Brunner, A. Prescimone, E. C. Constable and C. E. Housecroft, *Crystals*, 2020, **10**, 1, DOI: **10.3390/cryst10010001**.
67 Y. Ma, Y. F. Dong, P. F. She, S. J. Liu, M. J. Xie, Y. X. Yu, Y. H. Li, Q. Zhao and W. Huang, *Adv. Opt. Mater.*, 2018, **6**, 1801065, DOI: **10.1002/adom.201801065**.
68 G. U. Mahoro, E. Fresta, M. Elie, D. di Nasso, Q. Zhang, J.-F. Lohier, J.-L. Renaud, M. Linares, R. Wannemacher, J. Cabanil-las-Gonzalez, R. D. Costa and S. Gaillard, *Dalton Trans.*, 2021, **50**, 11049–11060, DOI: **10.1039/D1DT01689J**.
69 D. Cremer and J. A. Pople, *J. Am. Chem. Soc.*, 1975, **97**, 1354–1358, DOI: **10.1021/ja00839a011**.
70 C. R. Groom, I. J. Bruno, M. P. Lightfoot and S. C. Ward, *Acta Cryst*, 2016, **B72**, 171–179, DOI: **10.1107/S2052520616003954**.
71 A. Pintado-Alba, H. de la Riva, M. Nieuwhuyzen, D. Bautista, P. R. Raithby, H. A. Sparkes, S. J. Teat, J. M. López-de-Luzuriaga and M. C. Lagunas, *Dalton Trans.*, 2004, 3459–3467, DOI: **10.1039/B410619A**.
72 B. Deb, P. P. Sarmah and D. K. Dutta, *Eur. J. Inorg. Chem.*, 2010, 1710–1716, DOI: **10.1002/ejic.200901101**.
73 J. Yuasa, M. Dan and T. Kawai, *Dalton Trans.*, 2013, **42**, 16096–16101, DOI: **10.1039/C3DT51390D**.
74 C. Pelizzi and G. Pelizzi, *Acta Cryst*, 1979, **B35**, 1785–1790, DOI: **10.1107/S0567740879007779**.
75 E. R. T. Tiekink, *Z. Kristallogr. NCS*, 2001, **216**, 69–70, DOI: **10.1524/ncrs.2001.216.14.69**.
76 M. Llunell, D. Casanova, J. Cirera, P. Alemany and S. Alvarez, *SHAPE V. 2.1*, Universitat de Barcelona and University of Jerusalem, Barcelona, 2013.
77 J. Cirera, P. Alemany and S. Alvarez, *Chem. – Eur. J.*, 2004, **10**, 190–207, DOI: **10.1002/chem.200305074**.
78 S. Alvarez, P. Alemany, D. Casanova, J. Cirera, M. Llunell and D. Avnir, *Coord. Chem. Rev.*, 2005, **249**, 1693–1708, DOI: **10.1016/j.ccr.2005.03.031**.
79 L. Yang, D. R. Powell and R. P. Houser, *Dalton Trans.*, 2007, 955–964, DOI: **10.1039/B617136B**.
80 A. Okuniewski, D. Rosiak, J. Chojnacki and B. Becker, *Polyhedron*, 2015, **90**, 47–57, DOI: **10.1016/j.poly.2015.01.035**.
81 W. L. F. Armarego and D. D. Perrin, *Purification of Laboratory Chemicals*, Butterworth-Heinemann, Oxford, 1996.

82 C. Bianchini, C. A. Ghilardi, A. Meli, S. Midollini and A. Orlandini, *Inorg. Chem.*, 1985, **24**, 924–931, DOI: 10.1021/ic00200a025.
83 G. J. Kubas, B. Monzyk and A. L. Crumblis, *Inorg. Synth.*, 1990, **28**, 68–70, DOI: 10.1002/9780470132593.ch15.
84 S. Xie, Z. Yan, Z. Li, Q. Song and M. Ma, *J. Org. Chem.*, 2018, **83**, 10916–10921, DOI: 10.1021/acs.joc.8b01587.
85 X.-K. Liu, C.-J. Zheng, M.-F. Lo, J. Xiao, Z. Chen, C.-L. Liu, C.-S. Lee, M.-K. Fung and X.-H. Zhang, *Chem. Mat*, 2013, **25**, 4454–4459, DOI: 10.1021/cm403318r.
86 Bruker, APEX3, SMART, SAINT, Bruker AXS Inc., Madison, Wisconsin, USA, 2015.
87 P. McArdle, *J. Appl. Crystallogr.*, 2017, **50**, 320–326, DOI: 10.1107/S1600576716018446.
88 G. M. Sheldrick, *Acta Crystallogr.*, 2015, **A71**, 3–8, DOI: 10.1107/S2053273314026370.
89 G. M. Sheldrick, *Acta Crystallogr.*, 2015, **C71**, 3–8, DOI: 10.1107/S2053229614024218.
90 A. L. Spek, *Acta Crystallogr.*, 2020, **E76**, 1–11, DOI: 10.1107/S2056989019016244.
91 H. S. Yu, X. He, S. L. Li and D. G. Truhlar, *Chem. Sci.*, 2016, **7**, 5032–5051, DOI: 10.1039/C6SC00705H.
92 F. Weigend and R. Ahlrichs, *Phys. Chem. Chem. Phys.*, 2005, **7**, 3297–3305, DOI: 10.1039/B508541A.
93 M. Cossi, N. Rega, G. Scalmani and V. Barone, *J. Comput. Chem.*, 2003, **24**, 669–681, DOI: 10.1002/jcc.10189.
94 V. Barone and M. Cossi, *J. Phys. Chem. A*, 1998, **102**, 1995–2001, DOI: 10.1021/jp9716997.
95 C. A. Ullrich, *Time-dependent density functional theory*, Oxford University Press, Oxford, 2012.
96 M. J. Frisch, G. W. Trucks, H. B. Schlegel, G. E. Scuseria, M. A. Robb, J. R. Cheeseman, G. Scalmani, V. Barone, G. A. Petersson, H. Nakatsuji, X. Li, M. Caricato, A. V. Marenich, J. Bloino, B. G. Janesko, R. Gomperts, B. Mennucci, H. P. Hratchian, J. V. Ortiz, A. F. Izmaylov, J. L. Sonnenberg, D. Williams-Young, F. Ding, F. Lipparini, F. Egidi, J. Goings, B. Peng, A. Petrone, T. Henderson, D. Ranasinghe, V. G. Zakrzewski, J. Gao, N. Rega, G. Zheng, W. Liang, M. Hada, M. Ehara, K. Toyota, R. Fukuda, J. Hasegawa, M. Ishida, T. Nakajima, Y. Honda, O. Kitao, H. Nakai, T. Vreven, K. Throssell, J. A. Montgomery, Jr., J. E. Peralta, F. Ogliaro, M. J. Bearpark, J. J. Heyd, E. N. Brothers, K. N. Kudin, V. N. Staroverov, T. A. Keith, R. Kobayashi, J. Normand, K. Raghavachari, A. P. Rendell, J. C. Burant, S. S. Iyengar, J. Tomasi, M. Cossi, J. M. Millam, M. Klene, C. Adamo, R. Cammi, J. W. Ochterski, R. L. Martin, K. Morokuma, O. Farkas, J. B. Foresman and D. J. Fox, *Gaussian 16, Revision C.01*, Gaussian, Inc., Wallingford CT, 2016.
97 T. Lu and F. Chen, *J. Comput. Chem.*, 2012, **33**, 580–592, DOI: 10.1002/jcc.22885.